

Spring 1990

Initial characterization of coagulin polymerization and a novel trypsin inhibitor from *Limulus polyphemus*

Maribeth Ann Donovan
University of New Hampshire, Durham

Follow this and additional works at: <https://scholars.unh.edu/dissertation>

Recommended Citation

Donovan, Maribeth Ann, "Initial characterization of coagulin polymerization and a novel trypsin inhibitor from *Limulus polyphemus*" (1990). *Doctoral Dissertations*. 1608.
<https://scholars.unh.edu/dissertation/1608>

This Dissertation is brought to you for free and open access by the Student Scholarship at University of New Hampshire Scholars' Repository. It has been accepted for inclusion in Doctoral Dissertations by an authorized administrator of University of New Hampshire Scholars' Repository. For more information, please contact nicole.hentz@unh.edu.

INFORMATION TO USERS

The most advanced technology has been used to photograph and reproduce this manuscript from the microfilm master. UMI films the text directly from the original or copy submitted. Thus, some thesis and dissertation copies are in typewriter face, while others may be from any type of computer printer.

The quality of this reproduction is dependent upon the quality of the copy submitted. Broken or indistinct print, colored or poor quality illustrations and photographs, print bleedthrough, substandard margins, and improper alignment can adversely affect reproduction.

In the unlikely event that the author did not send UMI a complete manuscript and there are missing pages, these will be noted. Also, if unauthorized copyright material had to be removed, a note will indicate the deletion.

Oversize materials (e.g., maps, drawings, charts) are reproduced by sectioning the original, beginning at the upper left-hand corner and continuing from left to right in equal sections with small overlaps. Each original is also photographed in one exposure and is included in reduced form at the back of the book.

Photographs included in the original manuscript have been reproduced xerographically in this copy. Higher quality 6" x 9" black and white photographic prints are available for any photographs or illustrations appearing in this copy for an additional charge. Contact UMI directly to order.

U·M·I

University Microfilms International
A Bell & Howell Information Company
300 North Zeeb Road, Ann Arbor, MI 48106-1346 USA
313/761-4700 800/521-0600

Order Number 9027427

**Initial characterization of coagulin polymerization and a novel
trypsin inhibitor from *Limulus polyphemus***

Donovan, Maribeth Ann, Ph.D.

University of New Hampshire, 1990

Copyright ©1990 by Donovan, Maribeth Ann. All rights reserved.

U·M·I

300 N. Zeeb Rd.
Ann Arbor, MI 48106

**INITIAL CHARACTERIZATION OF COAGULIN POLYMERIZATION
AND A NOVEL TRYPSIN INHIBITOR FROM *LIMULUS POLYPHEMUS***

BY

**Maribeth A. Donovan
B.S., Providence College, 1985**

Dissertation

**Submitted to the University of New Hampshire
in Partial Fulfillment of
the Requirements for the Degree of**

Doctor of Philosophy

in

Biochemistry

May, 1990

ALL RIGHTS RESERVED

c 1990

Maribeth A. Donovan

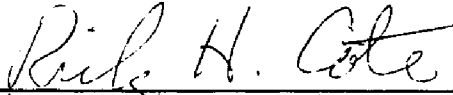
This dissertation has been examined and approved.



Dissertation director, Thomas M. Laue
Associate Professor of Biochemistry



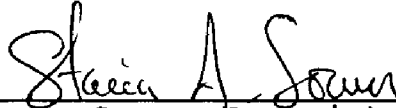
Andrew P. Laudano, Assistant Professor
of Biochemistry



Rick H. Cote, Assistant Professor of
Biochemistry



Thomas G. Pistole, Professor of
Microbiology



Stacia A. Sower, Associate Professor of
Zoology

07 MAY 1990
Date

Dedicated to the Memory of Margaret West Donovan

Acknowledgements

First and foremost I must thank Thomas M. Laue for his guidance, advice and patience. Most of all I am appreciative of his enthusiasm for biochemistry, teaching, learning, softball, and life in general. He is indeed a great motivator and it was my privilege to work for him.

Secondly, I must thank one of the other important men in my life. My father, Lawrence G. Donovan has been behind all of my endeavors. He may live in Illinois, but he is always there for me, financially and emotionally. Thanks Dad.

At this point I should mention those folks who helped with different aspects of this dissertation. The following people have my heart-felt thanks (listed in no apparent order): Elizabeth A. Luckow-Nichols, Paul Matsudaira, Dr. Norman Wainwright, David "gsplot" Hayes, Carol "the amino acid analyzer lady" Macomber, Daryl "I love the plate reader" Lyons, Terry "the sed velocity queen" Ridgeway, and Bob "let's bleed those crabs" Millham. I am grateful to the university for support in the form of a summer fellowship for TAs, two CURF grants and a dissertation year fellowship.

I can not thank enough my friends and relatives who have fed me, entertained me, and done my laundry for all these years of college and graduate school. Some are named above, some know who you are, and two I would like to mention by

name. Dr. and Mrs. Laurent Gousie have been my second set of parents since the days of Providence College. I am grateful to them for more than I can possibly list here.

Spike thanks the members of the biochemistry softball team (past and present) and the other volleyball junkies for loads of fun. Terry, thanks for making me go to aerobics. Ann, thanks for the blue drinks and for supporting my Batman habit.

Last but not least, I must thank my best friend, Michael Gousie. He has been more than patient with me. He has been supportive and a great source of entertainment. I bet you never thought I would finish. Neither did I. Let's go get some hacked chicken.

TABLE OF CONTENTS

DEDICATION.....	iv
ACKNOWLEDGEMENTS.....	v
LIST OF TABLES.....	ix
LIST OF FIGURES.....	x
ABSTRACT.....	xii
I. EFFECT OF PH ON THE SIZE DISTRIBUTION OF INTERMEDIATES IN <i>LIMULUS</i> COAGULIN POLYMERIZATION..	1
INTRODUCTION.....	2
MATERIALS.....	8
METHODS.....	9
Protein Preparation.....	9
Coagulin Polymerization/Depolymerization.....	9
Sedimentation Equilibrium.....	10
Sedimentation Velocity.....	12
Data Analysis.....	12
Estimation of Molecular Dimensions.....	15
Temperature Effect on Polymerization.....	19
RESULTS.....	20
Sedimentation Equilibrium Analysis of Coagulogen.....	20
Sedimentation Velocity Analysis of Coagulogen.....	21
Molecular Dimensions of Coagulogen.....	21
Coagulin Polymerization Reaction.....	24
Depolymerization of Gelled Coagulin.....	24
Sedimentation Velocity Analysis at Various pHs.....	27
Intermediates at pH 2.5.....	27
Molecular Dimensions of Coagulin.....	33
Evidence for Pressure Induced Polymerization.....	33
Evidence for Pressure Induced Depolymerization.....	36
Temperature Effect on Polymerization....	40

TABLE OF CONTENTS continued

DISCUSSION.....	43
Coagulogen and Pre-gel Species.....	43
Fiber and Gel Assembly.....	44
Effect of pH.....	46
Effect of Temperature.....	47
Effect of Pressure.....	48
Summary.....	52
II. PURIFICATION AND PARTIAL CHARACTERIZATION OF A NOVEL TRYPSIN INHIBITOR FROM THE HEMOLYMPH OF THE HORSESHOE CRAB <i>LIMULUS POLYPHEMUS</i>	53
INTRODUCTION.....	54
MATERIALS.....	56
METHODS.....	57
Protein Preparation.....	57
Clotting Assays.....	57
Protein Determination.....	58
Amino Acid Analysis of LTI.....	58
Amino-terminal Amino Acid Sequence of LTI...	58
Sedimentation Equilibrium.....	59
Proteinase Assays.....	60
RESULTS.....	63
Identification of an Inhibitor of Coagulogen Polymerization.....	63
Isolation of the Inhibitory Factor.....	68
Initial Characterization of LTI.....	68
Amino Acid Content.....	71
Amino-terminal Amino Acid Sequence.....	73
Sedimentation Equilibrium Analysis.....	74
Specificity of LTI.....	75
DISCUSSION.....	78
APPENDIX A.....	81
APPENDIX B.....	84
APPENDIX C.....	91
LIST OF REFERENCES.....	92

LIST OF TABLES

1.	Amino Acid Composition of the <i>Limulus</i> Trypsin Inhibitor (LTI).....	72
2.	Effect of LTI (7.9 μM) on Different Proteolytic Enzymes Using Casein (62 μM) as Substrate.....	76

LIST OF FIGURES

1.	A Proposed Mechanism for <i>Limulus polyphemus</i> blood Coagulation.....	4
2.	Movement of the Coagulogen Boundary with Time.....	23
3.	A Typical Coagulin Polymerization Reaction.....	26
4.	Depolymerization of Gelled Coagulin with Acid.....	26
5.	Coagulin Gel Intermediates at pH 2.5.....	29
6.	Movement of the Coagulin Boundary with Time.....	32
7.	Pressure-induced Polymerization of Coagulin Monomers at pH 4.6.....	35
8.	The Affect of Cyclooctane on Polymerization of Coagulin.....	38
9.	The Effect of Temperature on the Polymerization of Coagulin.....	42
10.	Elution profile of acid-treated <i>Limulus polyphemus</i> (Lp) hemolymph from a Sephadex G-50 column.....	65
11.	Trypsin-catalyzed polymerization of two different Lp coagulogen preparations.....	65
12.	Addition of aliquots of the unclottable G-50 Sephadex elution peaks had no effect on the polymerization reaction.....	67
13.	The effects of the removal of LTI from coagulogen on the trypsin-mediated polymerization reaction....	67
14.	SDS-PAGE of LTI eluted from the carboxymethyo-Sephadex column.....	70
15.	The Basic Elements of Sample Detection for an Analytical Ultracentrifuge.....	87
16.	View of a Double Sector Cell and a Cross-section of a Sample Sector.....	87
17.	Absorbance Scans of a Sedimentation Velocity Experiment of Coagulin at pH 2.5.....	89

LIST OF FIGURES continued

18. A Plot of the Ratio of the Experimental Frictional Coefficient and the Theoretical Frictional Coefficient (f/f_0) Versus the Axial Ratio..... 91

ABSTRACT

INITIAL CHARACTERIZATION OF COAGULIN POLYMERIZATION AND A NOVEL TRYPSIN INHIBITOR FROM *LIMULUS POLYPHEMUS*

by

Maribeth A. Donovan

University of New Hampshire, May, 1990

In the final step of coagulation in the horseshoe crab, coagulogen ($M_w = 19,000$, from sedimentation equilibrium) is converted by discrete proteolysis into its clottable form, coagulin. Coagulogen does not have a strong tendency to self-associate. In 0.1 M ammonium bicarbonate, 50 mM Tris-HCL (pH 8.1), trypsin generated coagulin rapidly associates to form a stable, solid gel. Polymerization is pH-dependent, with reversible depolymerization occurring in acid (midpoint pH 5.4). Sedimentation velocity analysis reveals that stable intermediates remain at pH 2.5, with 30-31 s being the predominant form along with monomer (1.89 s) and larger forms (>60 s). Near the midpoint of the titration, a pressure-dependent association occurs with a distribution of very large species resulting. There is also evidence that at this point a concurrent pressure-dependent depolymerization is occurring.

Trypsin inhibitory activity from the hemolymph of *Limulus polyphemus* was found to co-purify with coagulogen in the preparations. *Limulus* trypsin inhibitor (LTI) was separated from coagulogen by ion-exchange chromatography on

carboxymethyl-Sephadex. A molecular weight of 16,300 was determined by analytical ultracentrifugation. This value is consistent with estimates from SDS-PAGE and amino acid composition. The amino-terminal sequence consists primarily of hydrophobic amino acid residues. LTI was found to inhibit the action of trypsin on both high and low molecular weight substrates. It also inhibits chymotrypsin but has little or no effect on thrombin, thermolysin, pepsin, or papain. Comparison of the amino acid composition and amino-terminal sequence of LTI with those of other known trypsin inhibitors revealed no significant similarity to other trypsin inhibitors, suggesting it may represent a new class of proteinase inhibitors.

PART I

Effect of pH on the Size Distribution of Intermediates in
Limulus coagulin polymerization

INTRODUCTION

In the past few decades there has been considerable interest in the blood coagulation system in the horseshoe crab, *Limulus polyphemus* (Lp). Some of this interest stems from the observation by Levin and Bang (1) that the liquid material from Lp blood cells gels when exposed to bacterial endotoxin. Gram-negative bacteria can cause fever, hypotension, and intravascular coagulation in endotoxemic individuals (2). Lysates of Lp blood cells, therefore, have been used to detect the presence of endotoxins in the blood of patients infected with gram-negative bacteria (3) and in contaminated intravenous fluids (4). In an attempt to understand how endotoxins affect mammalian blood coagulation, researchers have been investigating the mechanism in Lp coagulation.

Lp blood, or hemolymph, contains one type of cell, the motile amebocyte. A typical amebocyte has an oval shape and contains all of the organelles found in an active cell. One Golgi apparatus is found in each cell. This complex gives rise to secretory vesicles which later fuse to form the major granules characteristic of the Lp amebocyte (5). These granules contain all of the factors required for blood coagulation in the animal (6).

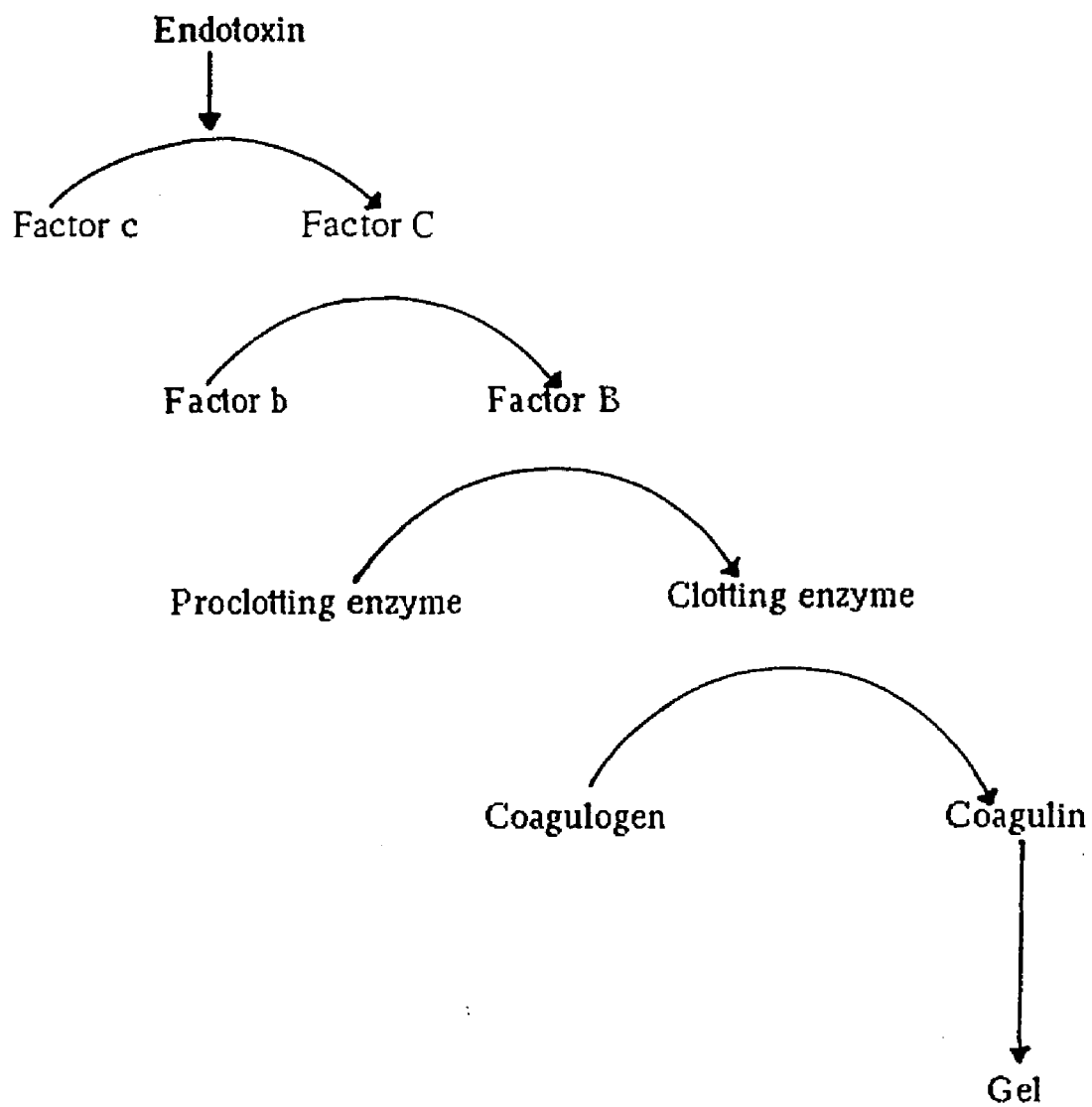
In the presence of endotoxin, amebocytes aggregate and

degranulate (7). This leads to the release of the blood coagulation factors. The coagulation system in Lp, like that in mammals, is controlled enzymatically (8). The granules contain serine proteinase zymogens whose sequential activation is endotoxin-initiated (9-14). Figure 1 illustrates a proposed mechanism for Lp hemocyte coagulation (12).

The final step of the coagulation cascade involves the limited proteolysis of coagulogen into its clottable form, coagulin (8). Coagulin monomers rapidly polymerize to form a gel or clot. One mode of protein self-association produces long rodlike structures whose final form depends on the surrounding conditions, including pH. Electron microscopic studies of coagulin gels dissolved at several pHs indicate the presence of helical fibers (15). The formation of the three-dimensional gel presumably involves the lateral association or aggregation of the fibers.

Polymerization resulting in long rodlike structures occurs via one of two pathways: a simple linear polymerization or a two-stage nucleated polymerization. A linear polymerization is characterized by an isodesmic association of monomeric units. Each sequential addition of monomer to the growing chain produces the same free energy change (16). This type of assembly process is not cooperative. A two-stage nucleated polymerization has been described as an assembly process consisting of two sequential linear polymerizations (16). For a system consisting of a one-dimensional assembly,

Figure 1. A Proposed Mechanism for Limulus polyphemus Blood Coagulation



the first linear polymerization serves to create a nucleus which then undergoes a second linear polymerization resulting in the formation of the larger helical structure. Both reactions can be isodesmic, however, there must be a difference in the free energy change between the two stages. The free energy change associated with the addition of monomers in the elongation stage is more negative than that associated with nucleation. The nucleation stage with its smaller free energy change is the rate limiting step, once the process is triggered, and it must occur first. Monomers associating with a growing helix make more or stronger contacts with the structure than do monomers forming the nucleus (17,18). Therefore, the association constant for elongation of a preformed nucleus is greater than that for nucleus formation. This allows the assembly process to be cooperative. Overall, the extent of helix formation is sigmoidal with time and is highly dependent on protein concentration. For a polymerization reaction which occurs in more than one dimension, the two stages of assembly may correspond to growth along different axes. The first stage would be the formation of fibers. The second stage would involve lateral aggregation of the fibers into a gel (19).

A gel, like that produced by coagulin self-assembly, is the result of a three-dimensional polymerization process. It can be defined as a lyophilic or solvent-loving colloidal system (20). The gel is a suspension of aggregated particles

in a continuous medium. In biological systems, in order to form a gel or clot, the fibers must associate into a network with space in between the molecules. Because solvent molecules are trapped in the interstices of the network, these molecules become oriented with respect to the protein. The strong, favorable protein-solvent interactions produced by the solvent ordering give stability to the gel.

The formation of a gel requires more contact points per monomer than does the formation of a linear or helical polymer. In addition to the contacts necessary to build a fiber, the monomers must have sites for lateral interactions with other fibers. One of the few biological systems that forms a gel is the fibrin assembly process at the end of the mammalian blood coagulation cascade. Fibrin monomers self-associate to form two-stranded rod-like structures (21,22) called protofibrils. The monomers are arranged in a staggered overlapping fashion with about 6 contacts per fibrin molecule (23). At a certain fiber length (600-800 nm in 0.1 M NaCl (19)), the protofibril has acquired the number of contacts needed to stabilize the lateral or protofibril-protofibril association which produces a thicker fibrin fiber (19,23). Complete gelation occurs when the outer surfaces of the protofibrils and/or the fibrin fibers are able to interact with other protofibrils or fibers. New contacts may not be necessary for the three-dimensional association. Instead, the network may be formed by protofibrils or fibrin fibers which

attach to more than one fibrin strand (19,23).

The association pathway for the coagulin gel is not known. Identifying intermediate species between monomeric and gelled coagulin will assist in the characterization of its mechanism of polymerization. The objective of this part of my dissertation is to detect and partially characterize stable intermediates in the coagulin gel assembly process. In the course of my investigation, I found a potent trypsin inhibitor co-purifying with coagulogen. Initial indications are that this inhibitor does not have an effect on Lp hemocyte clotting. It is therefore treated separately. The purification and partial characterization of the *Limulus* trypsin inhibitor (LTI) is described in Part II.

MATERIALS

Adult male horseshoe crabs were collected from Durham Point, New Hampshire or purchased from Marine Biological Laboratory, Woods Hole, Massachusetts. Sterile 30 and 60 cc syringes and 18 gauge needles were from Becton-Dickinson. Dialysis tubing (3500 molecular weight cutoff) was purchased from Spectrapor. Tubing closures were manufactured by Spectrum Medical Industries. Millipore immersible CX-10 single-use ultrafiltration units were used for protein concentration. Pharmacia supplied fine grade G-50 Sephadex and carboxymethyl-Sephadex (bead size 40-120 μm). N,N,N',N' tetramethylethylenediamine and low molecular weight gel electrophoresis standards were purchased from Biorad. N,N methylenebisacrylamide and Coomassie Brilliant Blue G-250 were obtained from Kodak. Equilibrium sedimentation data were gathered using Kodak technical pan film with an estar-AH base.

Cyclooctane was purchased from Sigma. Becton-Dickinson sterile tuberculin 1 cc, 26 gauge, 3/8 inch syringes were used to load the sedimentation velocity cells for non-cyclooctane runs. A Fisher-brand hypodermic 1 cc glass syringe with a 25 gauge needle was used to load cyclooctane. Reagent grade solution components were supplied by Baker.

METHODS

Protein Preparation

Limulus polyphemus coagulogen was purified essentially by the procedure described by Shishikura *et al* (24) (See Appendix A). Two ion exchange separations were added to the protocol. A carboxymethyl-Sephadex column was used to separate coagulogen from a trypsin inhibitor (Methods, Part II). Coagulogen in 0.1 M ammonium bicarbonate, pH 8.1 was incubated with diethylaminoethyl-Sephadex to remove any residual contaminants. Sephadex beads were removed by centrifugation. This was followed by passage of the coagulogen through a 0.22 μm filter to remove aggregates and dust. Purity was assessed by 10% sodium dodecyl sulfate polyacrylamide gel electrophoresis (SDS-PAGE) (25). Protein content was estimated using the absorbance at 280 nm assuming an extinction coefficient of 1 mg/ml \cdot cm.

Coagulin Polymerization/Depolymerization

Coagulogen can be converted *in vitro* into its polymerizable form, coagulin, by trypsin (26). Each polymerization assay contained 1 ml of filtered 50 mM Tris(hydroxymethyl)-aminomethane hydrochloride (Tris-HCl), pH 8.0 buffer, with and without 20 mM sodium acetate, and 0.5 ml of coagulogen (varied, see Results) (27). The reaction was initiated with

the addition of 0.02 ml of 1 mg/ml (final concentration 13 μ g/ml) trypsin in 0.001 N HCl (except where noted in the figure legend).

Solum (26) showed that "clotted" or polymerized coagulin can be dissolved in acid and then repolymerized when brought to an alkaline pH. Polymerized coagulin was depolymerized by the addition of aliquots of filtered HCl (0.1 or 1.0 N). The time courses of the polymerization and the depolymerization reactions were monitored by the change in absorbance at 320 nm. The spectrophotometer was zeroed at 320 nm with the coagulogen/Tris solution before the addition of trypsin.

Sedimentation Equilibrium

Sedimentation equilibrium experiments were conducted with a Beckman Model E analytical ultracentrifuge equipped with a temperature control, Rayleigh interference optics, an electronic speed control, and a 20 mW helium-neon laser light source (28). The temperature of the AN-D rotor was regulated at 23.3 °C. Analysis at 30,000 and 36,000 rpm were performed using a six-channel, 12-mm-thick, charcoal-filled epon centerpiece and sapphire windows.

Coagulogen (approximate concentration 263 μ g/ml) was dialyzed with three changes of 50 mM Tris, 0.1 M NaCl buffer, pH 7.6 (1:1000 vol:vol) at 4 °C for 72 h. Any particulates were removed by centrifugation in an Eppendorf microfuge at top speed for 5 min following dialysis. Dilutions were made

using the final dialysate.

High speed equilibrium experiments and blanks were carried out as described by Yphantis (29). Three sets of four interferogram exposure series were made at 30 min intervals after the estimated equilibrium time (29) had elapsed for each speed. 50 to 200 fringe displacements for each of five fringes were obtained from the interferograms at a radial spacing (in cell coordinates) of 50 μm near the meniscus, decreasing to 10 μm in high-gradient regions, using a Gaertner toolmaker's microscope (data kindly read by Daryl A. Lyons). Data were edited using REEDIT (kindly provided by David Yphantis). The reduced molecular weight (30) was estimated using nonlinear least squares analysis, NONLIN (31). The reduced apparent molecular weight, σ (cm^2), can be converted into the apparent weight-average molecular weight with the following equation (29):

$$M = \sigma RT [\omega^2 (1 - \bar{v} \rho)]^{-1} \quad \text{Equation 1}$$

where M = apparent weight-average molecular weight (g/mol)

\bar{v} = the partial specific volume (ml/g)

ρ = the density of the solution (g/ml)

ω^2 = the angular velocity squared (sec^{-2})

R = the gas constant (ergs/mol $^\circ\text{K}$)

T = the absolute temperature ($^\circ\text{K}$)

The association constant (K_a) for coagulogen self-association is returned from NONLIN as the natural logarithm of K_a (mm^{-1}). Conversion into the dissociation constant (K) and units of mM

was done as previously described (32).

Sedimentation Velocity

Sedimentation velocity experiments were performed as described by Chervenka (33) in a Beckman Model E analytical ultracentrifuge equipped with a temperature control, an electronic speed control, and a photoelectric scanner. Double sector, 12-mm-thick, aluminum-filled epon centerpiece and sapphire windows were used. Analyses were conducted at constant temperature: 20.5 °C for an AN-F rotor; 20.0 °C for an AN-H rotor. Absorbance (as a voltage) profiles of the cell image (scans) at 280 nm or 320 nm (to monitor scattering) were taken at several speeds during each run until the boundary(s) reached the bottom of the cell. Data were acquired from the scanner using an Analog/Digital converter interfaced to an IBM-PC microcomputer.

Data Analysis

The pressure inside the cell, due the gravitational field, increases from the air-liquid meniscus to the cell bottom (34). The pressure increases with radial position as $dP/dr = \rho\omega^2r$. The integral of this equation results in an equation that can be used to calculate the pressure at a given radial position:

$$P = P_0 + 1/2\rho\omega^2(r^2 - r_0^2) \quad \text{Equation 2}$$

where P_0 is the pressure at the meniscus position, r_0 and P is the pressure at the radial position r . Because of this

pressure gradient, the components in the solution at the base of the cell are under greater hydrostatic pressure than components closer to the meniscus.

The data for voltage as a function of time obtained from the scanner were converted to absorbance as a function of radial position as described by Chervenka (33).

Sedimentation of a particle in the centrifuge is due to the forces applied on the particle while the rotor is spinning (35). Particles in the rotor are subjected to three types of forces: (1) the centrifugal force, $F_c = m\omega^2r$, where m is the mass of the particle and ω^2r is the acceleration due to angular velocity ($\omega^2 = (2\pi\text{rpm}/60)^2$) and distance r from the center of rotation, (2) the force from the solution the particle is displacing as it moves, $F_b = -m_0\omega^2r$, where m_0 is the mass of the displaced solution, and (3) the frictional force, $F_d = -fv$, where f is the frictional coefficient and v is the velocity of the particle. The particle will reach a constant drift velocity when the sum of these forces is zero:

$$F_c + F_b + F_d = 0$$

or

$$m\omega^2r - m_0\omega^2r - fv = 0$$

The mass of the displaced solution, m_0 is equal to the product of the mass, the partial specific volume (\bar{v}) of the sedimenting particle and the density (ρ) of the buffer.

$$m\omega^2r - (m\bar{v}\rho)\omega^2r - fv = 0$$

Factoring out common terms results in:

$$m\omega^2r(1-\bar{v}\rho) - fv = 0$$

Since biomacromolecules are usually dealt with in terms of molar quantities, multiplication of this equation by Avogadro's number (N) will put the terms on a mole basis:

$$\omega^2rN(1-\bar{v}\rho) - Nfv = 0$$

The product of mass and Avogadro's number (mN) yields g/mol or molecular weight (M). Substituting M for mN and rearranging the equation, one is left with:

$$\omega^2rM(1-\bar{v}\rho) = Nfv$$

Rearranging once more, to separate variables from constants, results in an equation that will give us the sedimentation coefficient (s):

$$\frac{M(1-\bar{v}\rho)}{Nf} = \frac{v}{\omega^2r} = s \quad \text{Equation 3}$$

Put in words, the sedimentation coefficient (s) is equal to the velocity of the particle divided by the field strength. It is also proportional to the molecular weight and buoyancy of the particle and inversely related to the frictional coefficient of the particle.

From Equation 3, s can be determined experimentally as the ratio of the velocity of the particle to the force of the accelerating field. The velocity is calculated from the observed movement of a boundary (see Appendix B for an explanation of a boundary) with time: $v = dr_b/dt$, where r_b is the distance of the boundary from the center of rotation (radial position).

$$s = (\omega^2 r_b)^{-1} dr_b/dt$$

$$s\omega^2 r_b = dr_b/dt$$

$$s\omega^2 dt = dr_b/r_b$$

Integration of the last equation yields:

$$\omega^2 s(t-t^0) = \ln r_b - \ln r_b^0$$

where r_b is the boundary position at time t and r_b^0 is the boundary position at time t^0 . A graph of $\ln r$ vs t gives a straight line whose slope is $s\omega^2$. Linear regression can be used to determine the slope because the error in t is small compared to that in $\ln r$. In addition, the amount of experimental error is consistent and symmetrical for each data point. Since the rotor speed is known, ω^2 can be calculated and s can be determined. The units of s are seconds and 1×10^{-13} sec equals 1 Svedberg (s).

Sedimentation coefficient distributions ($G(s)$) were calculated as described by Williams *et al* (36). $G(s)$ is the integral distribution of the ratio of the concentration (or absorbance at 280 nm) at each s to the plateau concentration (or absorbance at 280 nm) in the cell. $G(s)$ gives the fraction of the sample having a value less than or equal to a given s . $g(s)$ is the derivative of the integral distribution, $G(s)$, with respect to s (i.e. $g(s) = dG(s)/ds$).

Estimation of Molecular Dimensions

The sedimentation coefficients of coagulogen and coagulin were calculated as described above. Corrections were made to

determine s at 20 °C in water (35):

$$s_{20,w} = \frac{(1-\bar{v}\rho)_{20,w}}{(1-\bar{v}\rho)_{20,b}} \cdot \frac{\eta_{20,b}}{\eta_{20,w}} \cdot s_{20,b}$$

Equation 4

The value for the viscosity ratio of 0.1 M ammonium bicarbonate to water ($\eta_{20,b}/\eta_{20,w}$) was estimated to be 1.012 (37). This value is the same for 50 mM Tris-HCl. The density (ρ) of water is 0.99823 g/ml and that of ammonium bicarbonate was estimated to be 1.0045 g/ml.

$s_{20,w}$ was then adjusted to zero concentration, $s_{20,w}^0$:

$$s_{20,w}^0 = s_{20,w}(1 + kC) \quad \text{Equation 5}$$

where C is protein concentration (g/l) and k is a constant with a typical value of 0.009 l/g (38). This corrects for the fact that with increasing concentrations the sedimenting particles will interfere with one another causing an increase in the frictional coefficient, f . From equation 3, it can be seen that s is inversely related to f . As the protein concentration increases, s will decrease for compact and extended macromolecules but will increase for reversibly associating particles (35).

With the corrected s ($s_{20,w}^0$) the experimental frictional coefficient can be calculated with equation 3:

$$f = \frac{M(1-\bar{v}\rho)}{Ns_{20,w}^0}$$

Molecular weight (M) and the partial specific volume (\bar{v}) are calculated (39) from the amino acid sequence of the protein.

The density (ρ) used is that of water.

To estimate the molecular dimensions of the particle, a model of an ellipsoid of revolution is assumed and the ratio of the axis lengths is determined. This axial ratio is estimated by comparing the experimental frictional coefficient of the particle (f) to a theoretical frictional coefficient (f_0) for a spherical particle.

$$f_0 = 6\pi\eta R \quad \text{Equation 6}$$

The viscosity (η) is that of water (0.01009 stokes). R is the stokes radius and is calculated from the volume of the particle:

$$\text{volume} = 4/3\pi R^3$$

The volume of a protein is dependent on the molecular weight (M), the partial specific volume (\bar{v}) and Avogadro's number (N): $\text{volume} = M\bar{v}/N$. Since proteins interact with the surrounding solvent, they invariably will have water molecules bound to internal cavities and as an external shell (40). This hydration phenomenon must be factored into the volume calculation as $(\bar{v} + \delta)$, where δ is the degree of hydration.

$$\text{volume} = M(\bar{v} + \delta)/N$$

For proteins with molecular weights less than 100,000, 0.280 g water per g protein is a good estimate for the degree of hydration (δ) (41).

Setting the two volume equations equal to one another allows for the determination of R :

$$M(\bar{v} + \delta)/N = 4/3\pi R^3$$

Rearranging:

$$R = [3M(\bar{V} + \delta)/4\pi N]^{1/3} \quad \text{Equation 7}$$

Once R is calculated from equation 7, f_0 can be determined with equation 6.

For a sphere, the major and minor radii (a and b, respectively) will be equal, therefore, the axial ratio a/b will be equal to 1. For an ellipsoidal particle, the major axis will be longer than the minor axis; the axial ratio a/b will be greater than 1. By comparing the experimental and theoretical frictional coefficients, the axial ratio of the particle can be estimated. If the particle is spherical, then $f = f_0$. The ratio of f/f_0 will be 1 indicating that $a = b$. With an f/f_0 greater than 1, the axial ratio can be determined from a graph of f/f_0 vs axial ratio (Appendix C) (42).

From the axial ratio a/b, the molecular dimensions of the particle can be calculated. For a prolate ellipsoid (cigar-shaped) the volume of the particle is equal to $4/3\pi ab^2$. Since the radii of the anhydrous particle is the desired value, the volume used in the calculation is that with a zero degree of hydration ($\delta=0$):

$$M\bar{V}/N = 4/3\pi ab^2 \quad \text{Equation 8}$$

With knowledge of the a/b ratio, one can substitute for one of the two variables:

$$a = (\text{axial ratio})b$$

$$M\bar{V}/N = 4/3\pi(\text{axial ratio})b^3$$

Solving for b:

$$b = [3M\bar{V}/4\pi N(\text{axial ratio})]^{1/3} \quad \text{Equation 9}$$

Multiplication of b (cm) by the axial ratio is a . Doubling a and b yields the axial lengths of the anhydrous particle.

Temperature Effect on Polymerization

The effect of changes in temperature on the coagulin depolymerization/polymerization reaction was studied in a Varian Cary 219 spectrophotometer equipped with a water-jacketed cuvette chamber. The coagulin clot was formed as previously described at room temperature using 50 mM Tris-HCl, 20 mM sodium acetate buffer, pH 8.0 and approximately 980 $\mu\text{g/ml}$ of coagulogen. After 30 min of clotting time, the gel was brought to pH 4.85 (approximately the dissolution midpoint) with HCl (1 and 0.1 N). The cuvette containing the depolymerized gel was placed in the spectrophotometer chamber at 23 °C. The temperature of the water bath was increased over a period of approximately 3 h. As the temperature in the chamber rose (toward 30.5 °C), the change in gel turbidity was monitored at 320 nm.

RESULTS

Sedimentation Equilibrium Analysis of Coagulogen

Before polymerization reactions can be studied, it is important to analyze the solution behavior of coagulogen. Sedimentation equilibrium was used to determine the reduced molecular weight of coagulogen and the tendency of coagulogen monomers to self-associate. The sedimentation equilibrium data from two solution samples (263 $\mu\text{g/ml}$, pH 7.6, 23.3 $^{\circ}\text{C}$) at two rotor speeds (30,000 and 36,000 rpm) were analyzed simultaneously, holding the second virial coefficient fixed at 0.003 mm^{-1} , to estimate the reduced molecular weight (σ) (30) and the association constant. This second virial coefficient is an estimate of nonideality and is typical for a slightly charged coagulogen molecule. The data were fit adequately by a model consisting of a single, weakly dimerizing component (the root mean square of the variance of the fit was 6.09 μm). Using σ (2.18 cm^{-2} with confidence limits of 2.15 to 2.22) and the partial specific volume (\bar{v}) calculated (39) from the amino acid composition (43), the apparent weight-average molecular weight of coagulogen (equation 1) is $19,000 \pm 300$ (the 65% confidence interval values returned by NONLIN were symmetrical and thus correspond to standard deviation). This molecular weight is in agreement with that expected from the amino acid sequence (19,674 g/mol)

(43). The dissociation constant determined from this analysis is 2.1 mM (1.3 to 3.7 mM) (values calculated from the data determined by NONLIN: -3.09 mm^{-1} (-3.65 to -2.61) (32)), indicating that coagulogen does not have a strong tendency to self-associate.

Sedimentation Velocity Analysis of Coagulogen

Coagulogen (283 $\mu\text{g/ml}$) in 0.1 M ammonium bicarbonate, pH 8.1 was analyzed by sedimentation velocity at 56,000 rpm and 20 °C in an AN-H rotor. Zero time was estimated at two-thirds of the final rotor speed (37,000 rpm) (33). A single boundary was observed. The movement of the radial position of the boundary with time was measured and a plot of $\ln r$ vs time was produced (Figure 2). From the slope of the line the apparent sedimentation coefficient was determined to be 2.1₆ s. Using a \bar{V} of 0.709₆ ml/g for coagulogen (in both water and buffer) s was corrected to water and zero protein concentration (equations 4 and 5) to give $s_{20,w}^0$ equals 2.2₂ s.

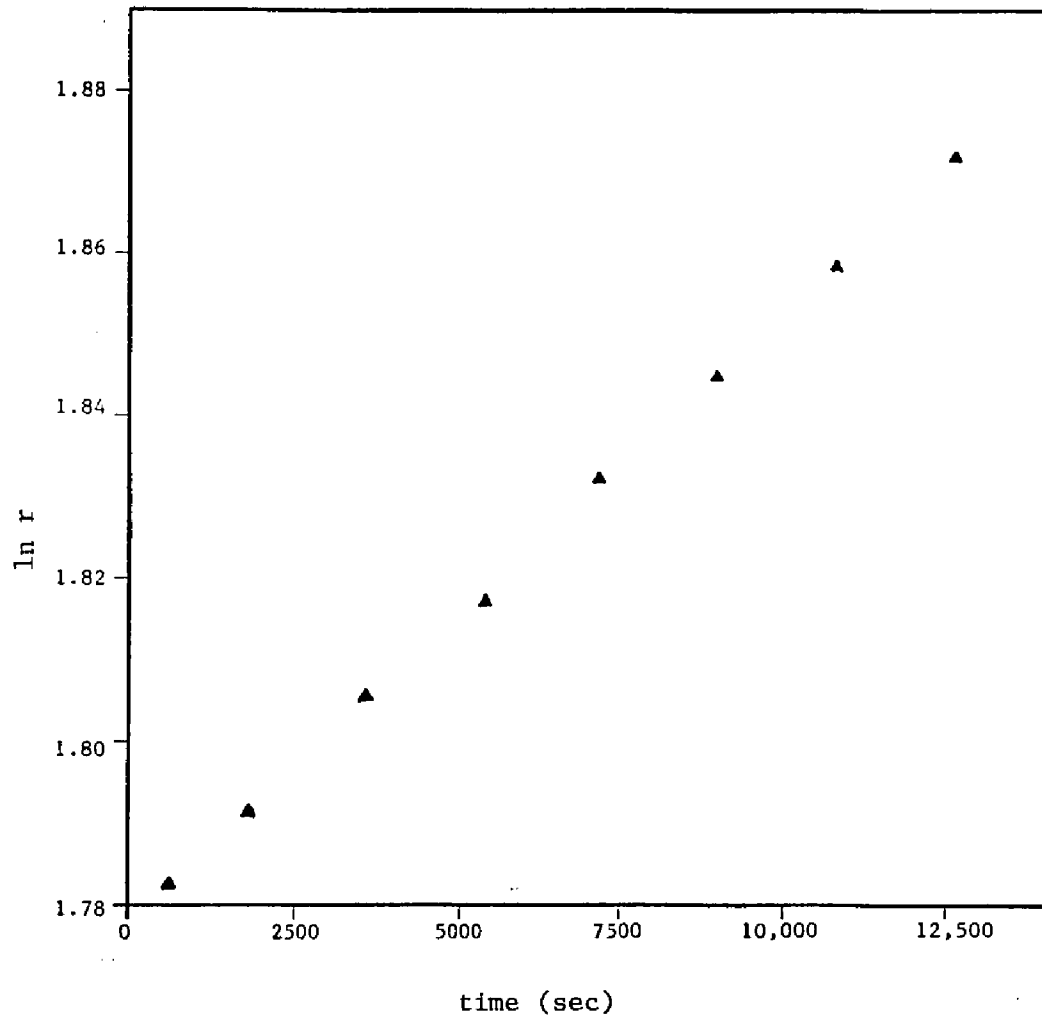
Molecular Dimensions of Coagulogen

From equation 3 (where $M = 19,674 \text{ g/mol}$ and $\bar{V} = .709_6 \text{ ml/g}$, both calculated from the amino acid composition (43)), the experimental frictional coefficient (f) for coagulogen is $4.28_{387} \times 10^{-8} \text{ g/sec}$. The stokes radius (R) of coagulogen, assuming $\delta = 0.280 \text{ g water/g protein}$, is $1.92_{077} \times 10^{-7} \text{ cm}$ (equation 7). Substituting in equation 6, the theoretical frictional coefficient (f_0) for a coagulogen sphere is 3.65_{315}

Figure 2:

Movement of the coagulogen boundary with time. Coagulogen (283 $\mu\text{g/ml}$) in 0.1 M ammonium bicarbonate, pH 8.1 was analyzed by sedimentation velocity at 56,000 rpm and 20 °C. The movement of the boundary with time was measured from several absorbance scans. The slope of this line is $s\omega^2$, where s is the apparent sedimentation coefficient and ω^2 is the angular acceleration. Using linear regression and the ω^2 for 56,000 rpm, the s for coagulogen is 2.1₆ s.

Figure 2.



$\times 10^{-8}$ g/sec. The ratio of the experimental and theoretical frictional coefficients, f/f_0 , is 1.173. Using Figure 18 from Appendix C, the axial ratio, a/b , for coagulogen is 3.8. Equation 9 allows for the calculation of the radii of anhydrous coagulogen. For a prolate ellipsoid coagulogen molecule, the dimensions (in terms of diameters) are 86 Å by 23 Å.

Coagulin Polymerization Reaction

Figure 3 illustrates the trypsin-mediated polymerization of coagulin (initial coagulogen concentration was approximately 740 $\mu\text{g/ml}$) as determined by the changes in turbidity. The increase in light scattering (increase in absorbance at 320 nm) is indicative of a large and growing structure. In other words, coagulin is polymerizing into a gel. In the first 2 min, the reaction is quite slow; this apparent lag phase is consistent with the coagulin polymerization reaction being a two-stage process.

Depolymerization of Gelled Coagulogen

At pH 8.1 the coagulin gel is semisolid and quite turbid (Figure 4). As aliquots of acid are added, the light scattering of the solution decreases. The shape of the dissolution curve is sigmoidal and the apparent titration midpoint is approximately pH 5 to 5.5.

Figure 3:

A typical coagulin polymerization reaction, initiated with 0.1 mg/ml trypsin in 0.001 N HCl (final trypsin concentration 1.3 μ g/ml), has a sigmoidal shape. The reaction contained 740 μ g/ml of coagulogen and was run at a pH of 8.1 and at room temperature (see Methods for details). After 109 min the turbidity of the solution was 0.102.

Figure 4:

Depolymerization of gelled coagulin with acid. Each trial contained approximately 350 μ g/ml of coagulogen and the titrations were carried out between 20 °C and 24 °C. Other elements of the reactions can be found in Methods.

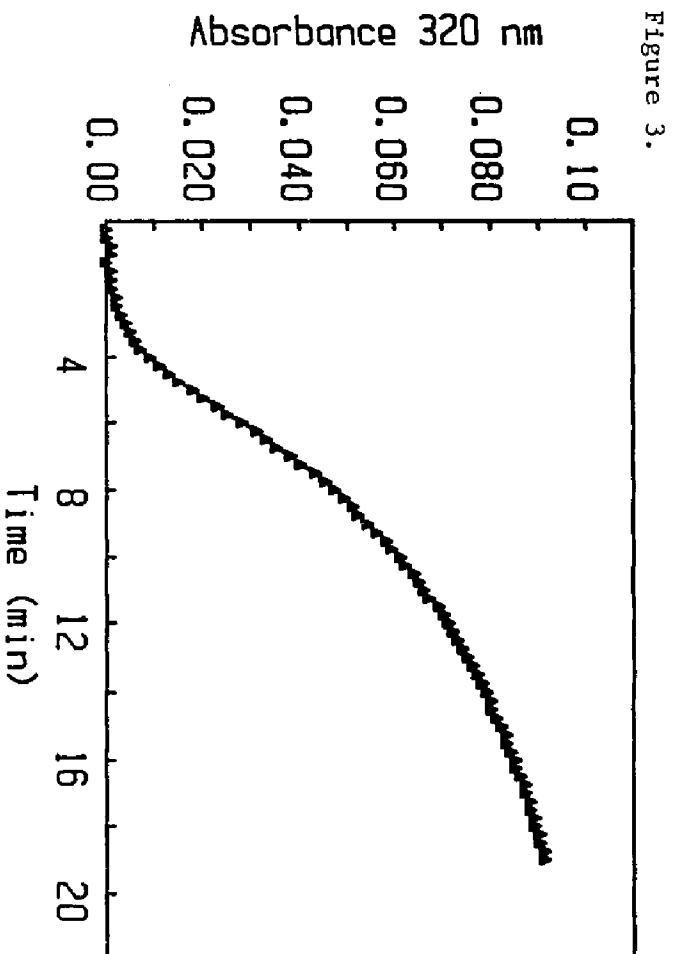
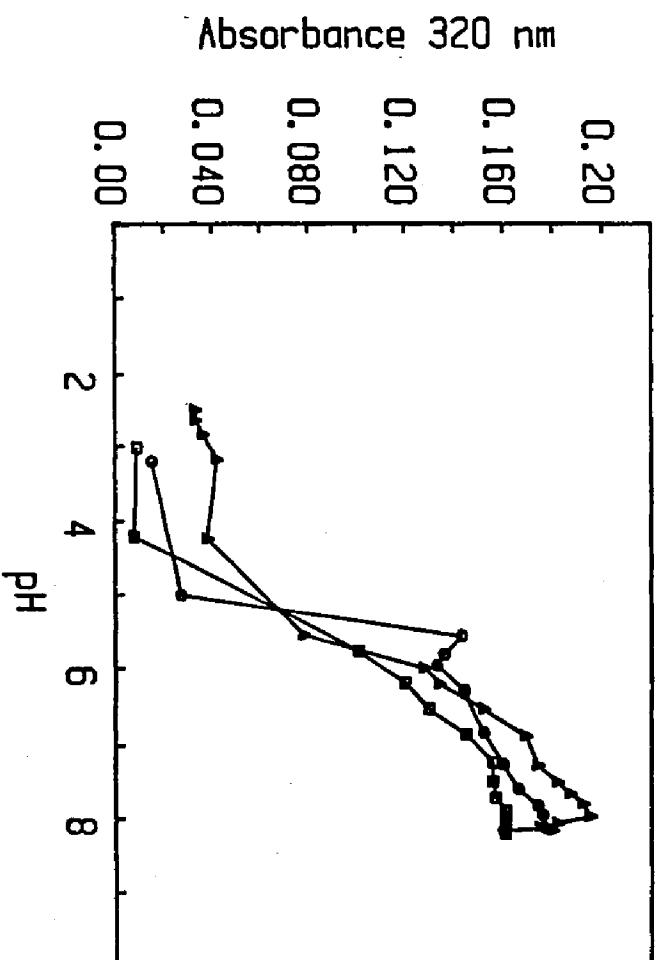


Figure 4.



Sedimentation Velocity Analysis at Various pHs

To identify possible intermediates in the coagulin polymerization process, sedimentation velocity experiments were conducted at various pHs. Below pH 4, the turbidity (Figure 4) is close to zero suggesting that larger scattering species are no longer present in the coagulin solution. Light scattering in the spectrophotometer is not be helpful in elucidating the presence of discrete stable species. To do this, sample fractionation is necessary. The technique chosen was sedimentation velocity analysis. An explanation of this technique, including unprocessed data, can be found in Appendix B.

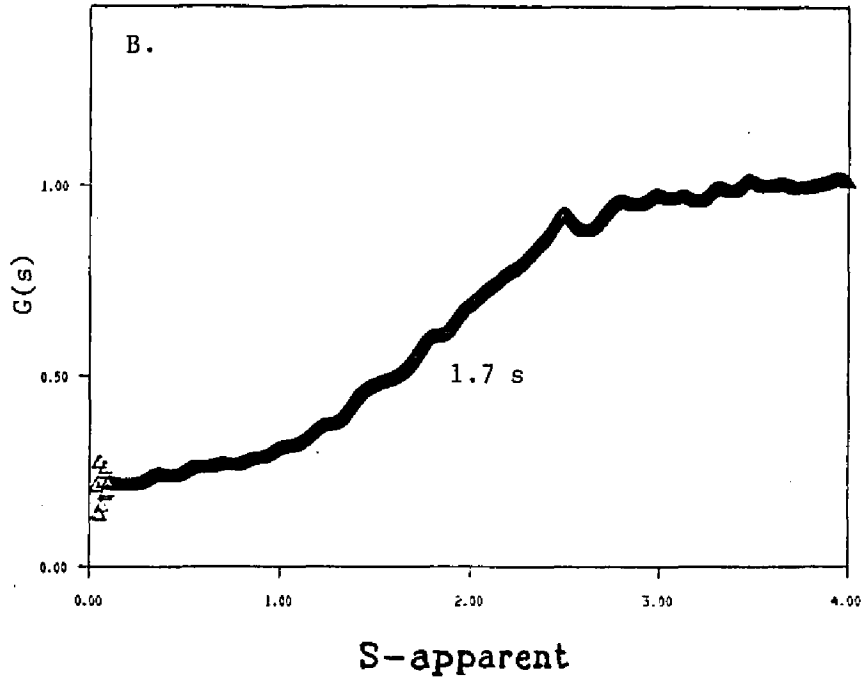
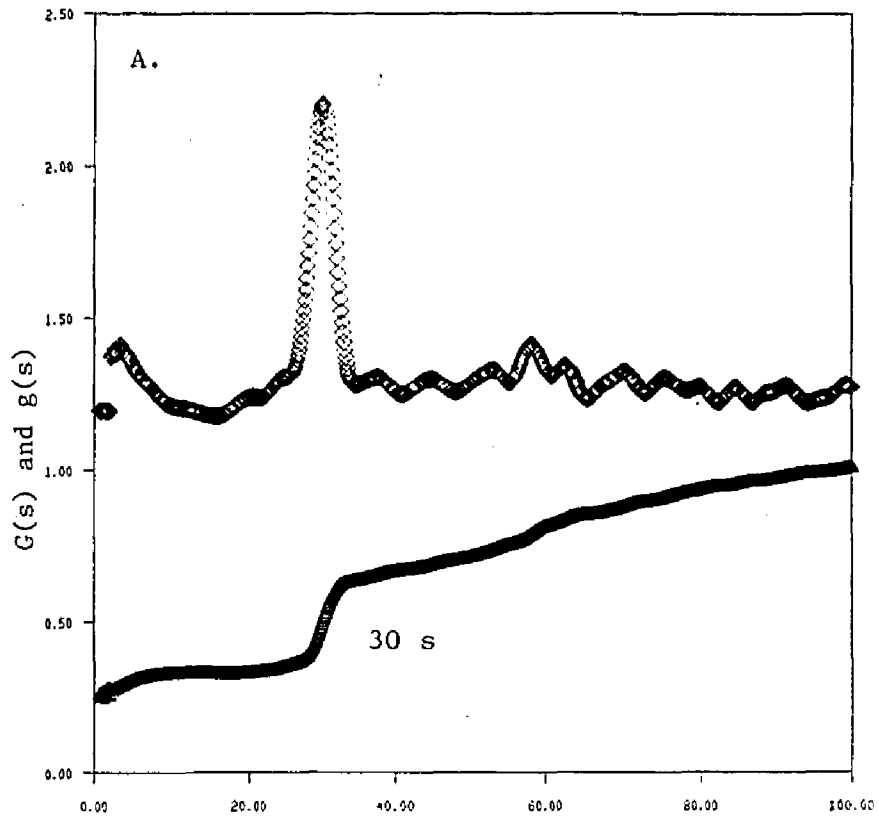
Intermediates at pH 2.5. Coagulogen (560 $\mu\text{g/ml}$) was treated with trypsin and the resulting coagulin was allowed to polymerize for 30 min (final turbidity = 0.282). HCl was added in aliquots until the pH reached 2.5. At this pH the turbidity (at 320 nm) of the solution was 0.008 indicating the dissolution of the gel. This solution was analyzed in the analytical ultracentrifuge in an AN-F rotor at 36,000 rpm.

Figure 5A is the sedimentation coefficient distribution calculated from an absorbance scan (280 nm) taken 1192 sec after the estimated zero time (two-thirds speed, 24,000 rpm) (33). The scan can be seen in Appendix B, Figure 15A. The triangles (lower curve) depict the integral $G(s)$. This curve reveals that approximately 48% of the particles in the coagulin solution have a sedimentation coefficient of 30 s or

Figure 5:

Coagulin gel intermediates at pH 2.5 were studied by sedimentation velocity. The initial coagulogen concentration was 560 $\mu\text{g/ml}$. The polymerization reaction (see Methods) was allowed to occur for 30 min before addition of HCl. G(s) analysis was used to determine apparent sedimentation coefficients. A: analysis at 36,000 rpm, lower trace is G(s), upper trace is g(s); B: analysis of solution in A at 56,000 rpm.

Figure 5.



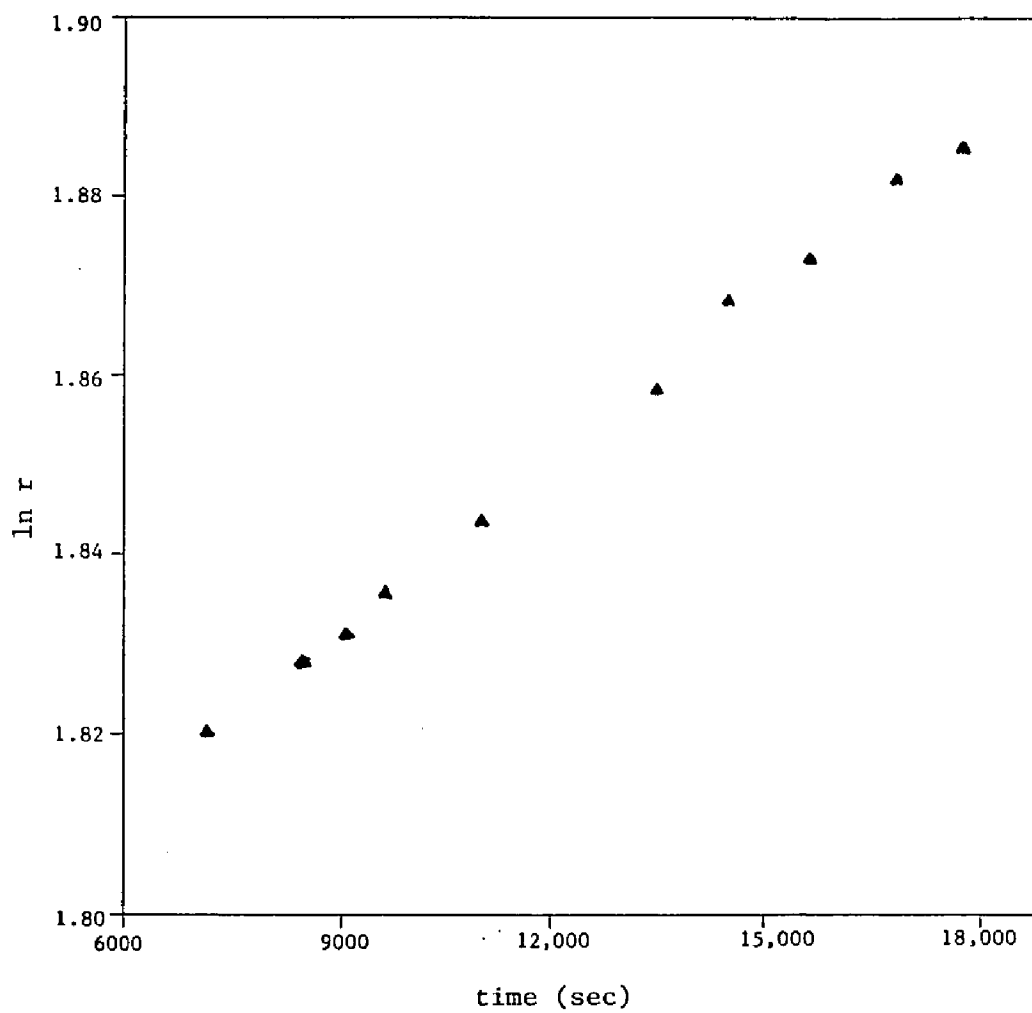
less. Approximately 30% of the solution has an s -apparent of 30 s. The $g(s)$ curve yields a peak at the midpoint of the boundary, whose position provides an estimate of the s -apparent. The slope in the plateau area of the $G(s)$ curve indicates the presence of species larger than 30 s. This could indicate a pressure-dependent reaction involving the 30 s material or the presence of stable, larger aggregates. A scan at 320 nm showed no increased solution turbidity from the meniscus to the cell bottom. Therefore, the larger particles are not the result of very large aggregates forming during the experiment. Heterogeneity of particles in the solution is the more probable cause of the sloped plateau.

In order to get an estimate of the sedimentation coefficient of the smaller coagulin species, the solution from Figure 5A was analyzed at a higher rotor speed. The solution was removed from the AN-F rotor, shaken vigorously, loaded in an AN-H rotor, and re-analyzed at 56,000 rpm. Figure 5B is the result of a $G(s)$ analysis of a scan at 280 nm at 12,022 sec from two-thirds speed (37,000). It indicates the presence of a species with an s -apparent of 1.7 s. When concentration vs s -apparent graphs of the data are compared, the concentration in the region below the 30 s boundary of Figure 5A is identical to that of the plateau region of Figure 5B, approximately 140 $\mu\text{g/ml}$ (data not shown). This indicates that the fraction of 1.7 s material remains constant over 18 h at room temperature.

Figure 6:

Movement of the coagulin boundary with time. Approximately 140 $\mu\text{g/ml}$ of coagulin were present in the pH 2.5 solution that was analyzed at 56,000 rpm. The movement of the boundary was measured from several absorbance scans. The slope of this line is $s\omega^2$, where s is the apparent sedimentation coefficient and ω^2 is the angular velocity. Using linear regression and the ω^2 for 56,000 rpm, the s for coagulin at pH 2.5 is 1.84 S.

Figure 6.



To get a better estimate of the sedimentation coefficient of coagulin at pH 2.5, the movement of the radial position of the boundary was measured and a plot of $\ln r$ vs time was produced (Figure 6). From the slope of the line, the apparent sedimentation coefficient was determined to be 1.8_4 s. Using a \bar{v} of 0.705 ml/g for coagulin (for water and buffer), s was corrected to water and zero concentration (equations 4 and 5) such that the $s_{20,w}^0$ is 1.8_{93} s. The coagulin concentration used in equation 5 (for zero concentration correction) was estimated from the fraction of the total coagulin solution with an s of 1.7 s (Figure 5A).

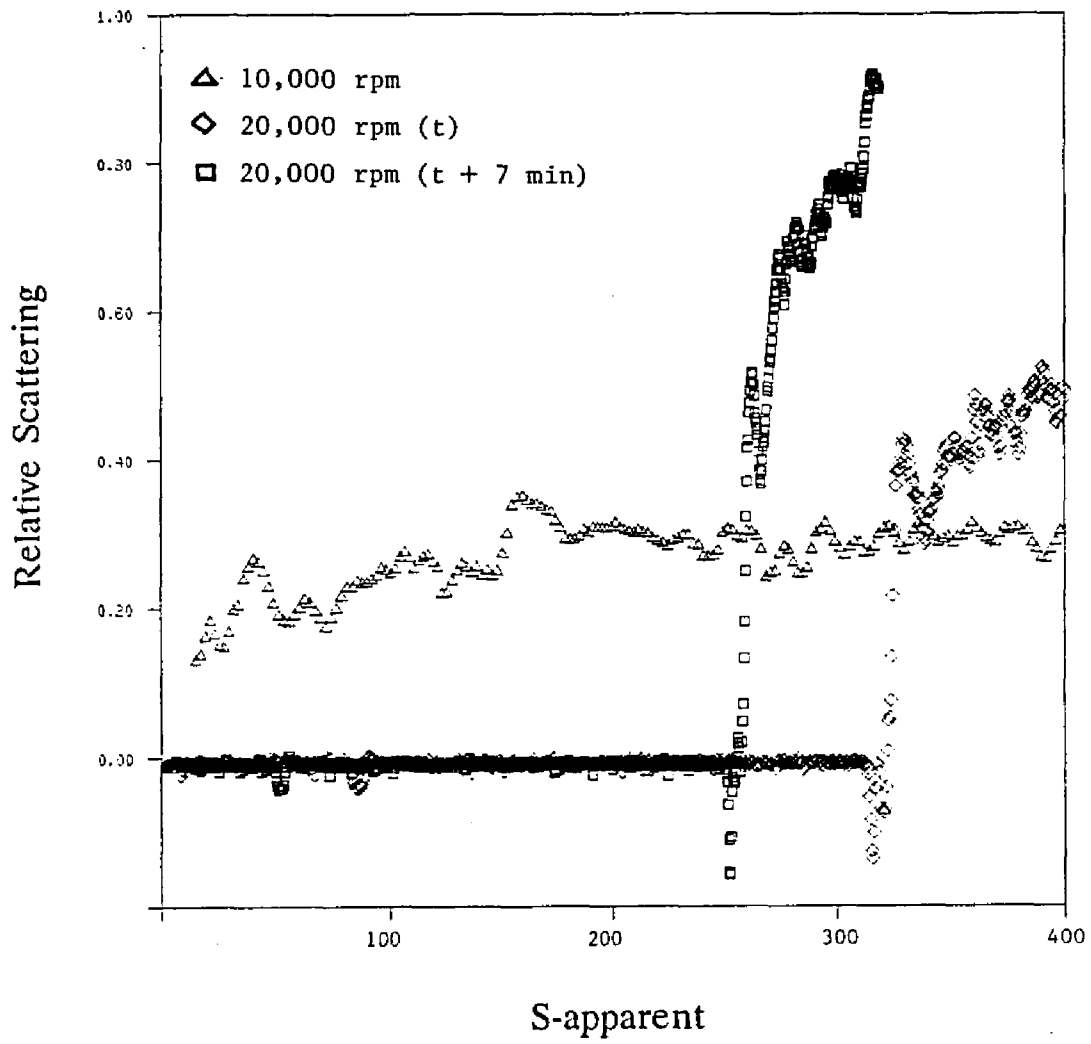
Molecular Dimensions of Coagulin at pH 2.5. From equation 3 (where $M = 16,792$ g/mol and $\bar{v} = .705$ ml/g), the experimental frictional coefficient (f) for coagulin at pH 2.5 is $4.36_{526} \times 10^{-8}$ g/sec. The stokes radius of coagulin, assuming $\delta = 0.280$ g water/g protein (equation 7) is $1.81_{8048} \times 10^{-7}$ cm. Substituting in equation 6, the theoretical frictional coefficient (f_0) for a coagulin sphere is $3.45_{778} \times 10^{-8}$ g/sec. The ratio of the experimental and theoretical frictional coefficients, f/f_0 , is 1.262. Using Figure 18 from Appendix C, the axial ratio, a/b , for coagulin at pH 2.5 is 5.2. Equation 9 allows for the calculation of the radii of an anhydrous coagulin monomer. For a prolate ellipsoid coagulin molecule, the diameter dimensions are 100 Å by 19 Å.

Evidence for Pressure-induced Polymerization. Coagulin at pHs just below the acid titration midpoint (Figure 4) were

Figure 7:

Pressure induces coagulin gel formation. A coagulin gel at pH 4.6 (810 $\mu\text{g/ml}$) was analyzed by sedimentation velocity at speeds of 10,000 (triangles) and 20,000 (diamonds and squares). The second scan at 20,000 (squares) was taken 7 min after the initial one (diamonds).

Figure 7.



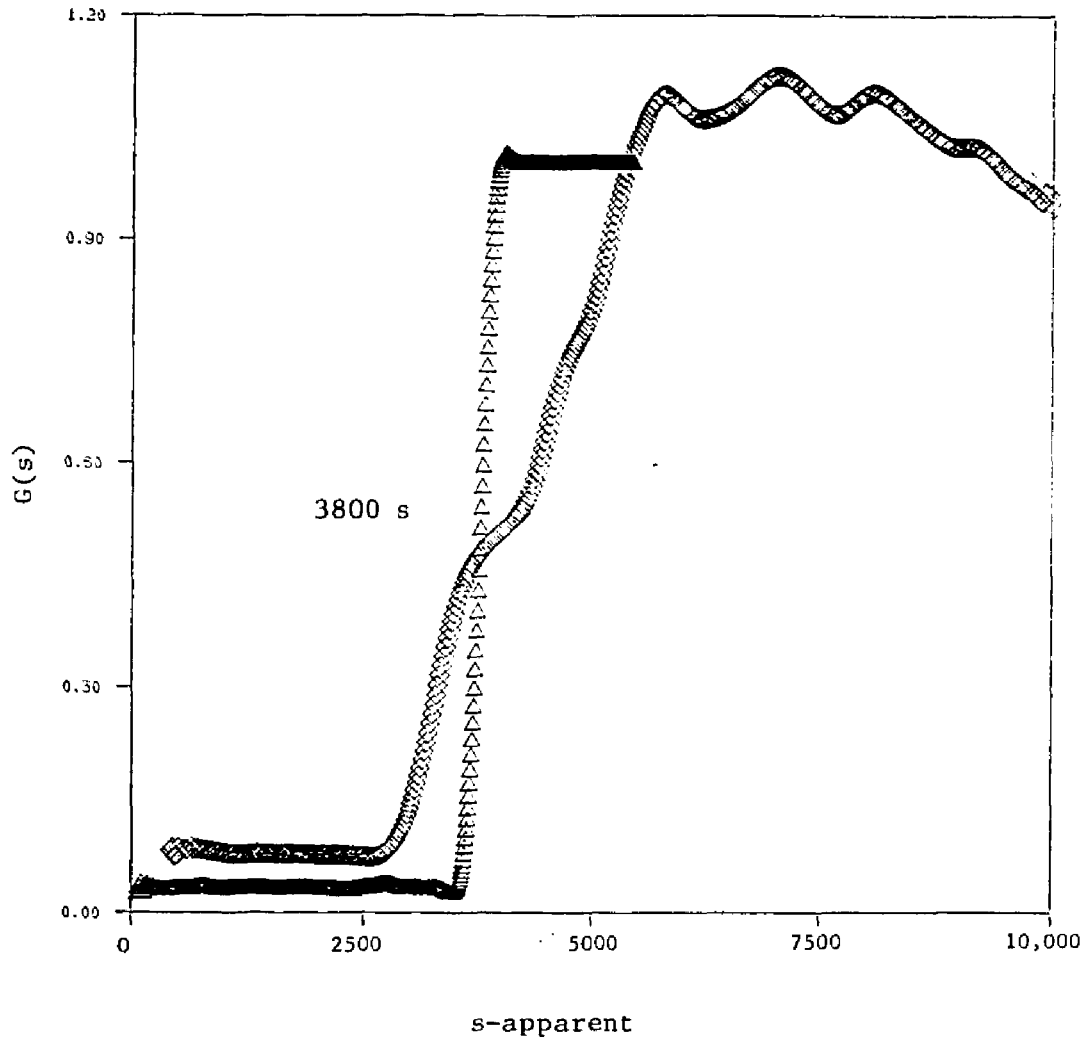
studied in order to assess the formation of stable species greater than 30 s. Before centrifugation, the coagulin solution (810 $\mu\text{g/ml}$, turbidity before acidification = 0.434) at pH 4.6 had an absorbance of 0.044 at 320 nm (determined spectrophotometrically). Figure 7 illustrates the relative scattering (absorbance at 320 nm) vs s-apparent of three scans. At 10,000 rpm (AN-F rotor) after 968 sec, there is no boundary apparent. However, the absorbance at 320 nm has increased (Figure 7, triangles) from the initial 0.044 to between 0.2 and 0.3 (less than the absorbance of 0.434 for the gel at pH 8.1). This solution was then brought to a rotor speed of 20,000 rpm. 919 sec after zero time for 20,000 rpm, a hyper-sharp boundary is visible and the solution turbidity increased even further (diamonds). Later (1339 sec), the boundary appears to slow down, and the turbidity continues to increase (squares). The increase in light scattering at the bottom of the cell and the apparent slowing down of the boundary are consistent with the sedimentation of a gel (44). Adding pressure, therefore, seems to favor the repolymerization of the coagulin gel.

Evidence for Pressure-induced Depolymerization. In order to further examine the effects of hydrostatic pressure on this apparently pressure-sensitive system, before the occurrence of any significant mass transport of particles, an immiscible substance was layered over a coagulin solution and analyzed at a low rotor speed (34). The solution with this inert

Figure 8:

The effect of cyclooctane on pressure-induced polymerization. Two aliquots of a pH 4.4 coagulin solution (421 $\mu\text{g/ml}$) were analyzed at 290 nm at 6400 rpm. One aliquot had cyclooctane layered over it (squares); one did not (triangles).

Figure 8.



substance, cyclooctane, would be subjected to a greater amount of hydrostatic pressure than a non-layered solution. Before centrifugation, the coagulin solution (421 $\mu\text{g/ml}$) at pH 4.4 had an absorbance of 0.048 at 320 nm (determined spectrophotometrically). Two aliquots of this solution were loaded into an AN-F rotor. One solution had an aliquot of cyclooctane (density = 0.835 g/ml) layered over it (Figure 8, squares). The other solution, without cyclooctane, served as a control. The $G(s)$ plots pictured in Figure 8 are from scans at 290 nm at 6400 rpm after 216 (squares) and 529 sec (triangles). For the solution without cyclooctane (triangles), the $G(s)$ analysis shows a species with an apparent s of 3800 S. At 6400 rpm the pressure at the base of the cell (4.29 atm) was enough to induce an increased turbidity, suggesting increased polymerization. However, with cyclooctane at its meniscus (and thus a cell bottom pressure of 4.84 atm), the coagulin solution behaved quite differently (squares) (both pressures were calculated with equation 2). Instead of a sharp boundary, a broader distribution of sedimentation coefficients can be observed with apparently more material with a higher s value. This, again, suggests pressure-induced polymerization. However, the decreasing scattering in the plateau region suggests that a rapid depolymerization also may be occurring in the solution. The noisiness is consistent with the presence of convection in the cell (44) which can be caused by a reaction taking place in the cell (34).

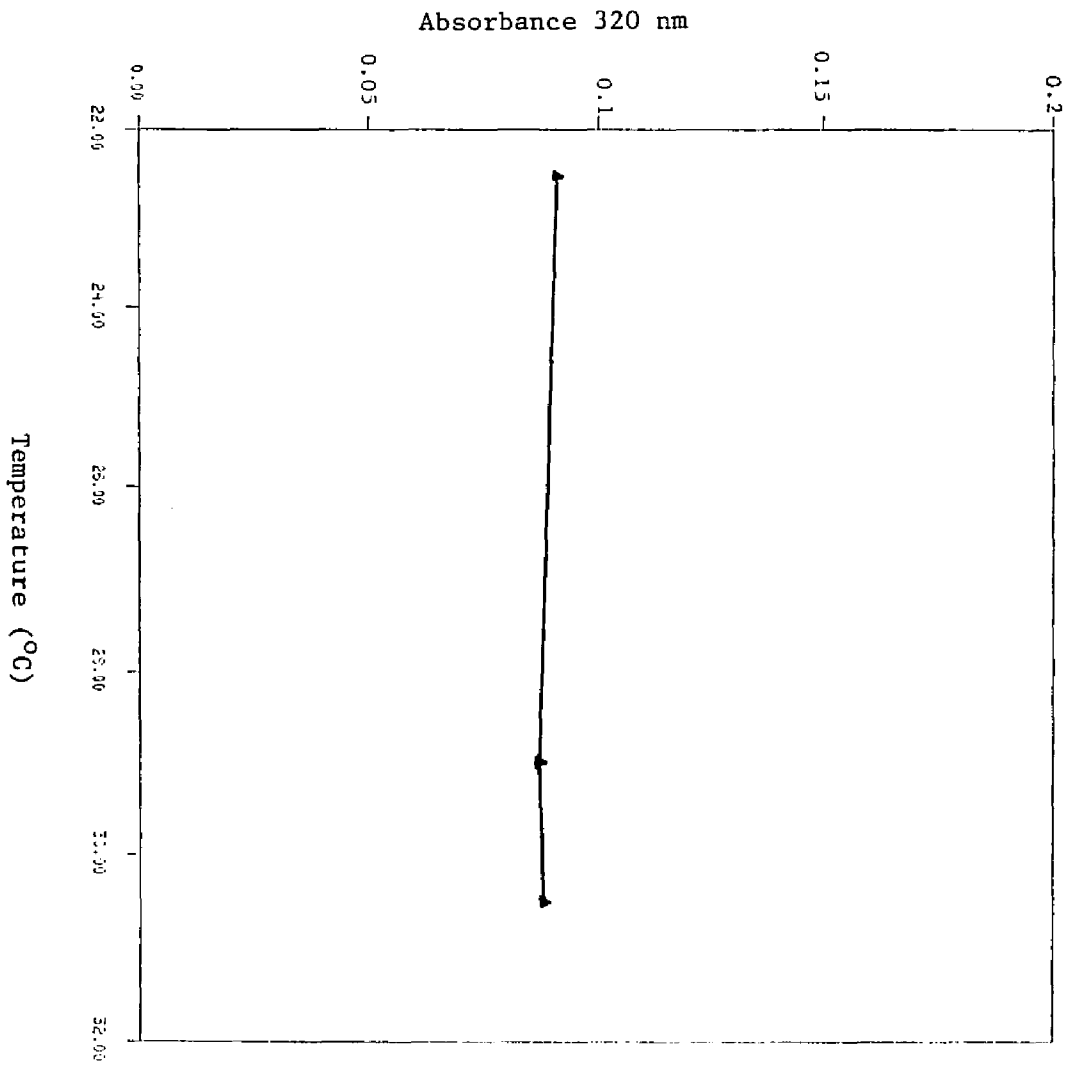
Temperature Effect on Polymerization.

To further examine the repolymerization phenomenon, the turbidity of a coagulin solution (975 $\mu\text{g/ml}$) at pH 4.85 was measured from 23 to 32.5 $^{\circ}\text{C}$. The purpose of this experiment is to determine whether or not polymerization is an enthalpically driven process. A coagulin gel solution dissolved to pH 4.85 (just below the titration midpoint) was unaffected by a slow increase in temperature (Figure 9).

Figure 9:

The effect of temperature on the polymerization of coagulin. A coagulin solution (initial coagulogen concentration was 975 $\mu\text{g/ml}$) was brought to pH 4.85 with acid. At 22.5 °C this solution had an absorbance at 320 nm of 0.091. The increase in temperature occurred in approximately 3 h. Buffer components are described in Methods.

Figure 9.



DISCUSSION

In response to the invasion of endotoxin (lipopolysaccharide) from Gram-negative bacteria, the blood coagulation system in the horseshoe crab, *Limulus polyphemus* (Lp), is triggered (1,7,8). In the ultimate catalytic step of the blood clotting cascade, coagulogen is converted into coagulin (8). This form of the protein is able to polymerize into a gel, thus sealing the infected wound in the injured animal. The objective of this part of my dissertation is the characterization of this polymerization reaction. Previous electron microscopy studies have indicated the presence of helical fibers in coagulin gels at low pHs (15). This investigation endeavored to identify stable intermediates and the mechanism by which they are formed.

Coagulogen and Pre-gel Species

Coagulogen is a single chain polypeptide composed of 175 amino acids (43). By sedimentation equilibrium, the molecular weight of coagulogen is 19,000. Because sedimentation equilibrium is a direct physical technique for determining molecular weight, this value is more accurate than the value estimated from SDS-PAGE (23,000) (26). My value is consistent with gel filtration data (19,500) (24) and with that expected from the amino acid sequence (19,674) (43).

Under the experimental conditions applied, coagulogen exhibited a weak self-association ($\Delta G'_{dis} = +3.6 \pm 0.3$ kcal/mol). Because of the high concentration of proteins in the granules of the amebocytes, however, one would suspect that some degree of association does occur *in vivo*. Otherwise, the osmotic pressure inside the granule might be very large.

Conversion of coagulogen into its clottable form, coagulin, involves the release of a 28 amino acid peptide (peptide C) from within the polypeptide chain (45). The liberation of this peptide apparently uncovers the contact sites necessary for fiber or gel formation. Coagulin sediments more slowly than its precursor form (1.8₀ s as compared to 2.2₂ s). Due to the loss of peptide C, it has a smaller molecular weight (16,792 from the amino acid composition (43)). Coagulin also has a slightly larger frictional coefficient than coagulogen (4.36×10^{-8} g/sec vs 4.28×10^{-8} g/sec), most likely due to the greater assymetry. The somewhat more expanded size for coagulin is consistent with unfolding of the molecule at pH 2.5. *In vivo*, however, coagulin would be at a more neutral pH (the pH of amebocyte lysates is 7.5 - personal communication of Dr. Norman Wainwright).

Fiber and Gel Assembly

Sedimentation velocity experiments have shown the

presence of a 30 s species at pH 2.5. Holme and Solum have observed apparently helical fibers at pH 3.0 with electron microscopy (15). According to their model, the periodicity of the helix is 45 to 50 Å. The diameter of the strand is 25 Å and the total helix diameter is 50 to 70 Å. Given a coagulin molecular weight of 17,000, they estimate one monomer per turn of the helix. The authors point out that given the limitations of the negative staining technique used, other models are possible. Assuming that the molecular dimensions of coagulogen determined in my study (86 by 23 Å) are closer to the dimensions of coagulin in the fiber than are the possibly denatured dimensions, a linear model can be constructed in accordance with the data of Holme and Solum. A plausible linear structural model is one similar to that of the fibrin protofibril (23). If we say that the coagulin molecule has two equal-sized lobes and that the monomers in a double-stranded fiber are arranged in a staggered overlapping fashion, we will get the following dimensions. The periodicity, from one lobe center to another, would be 43 Å. The diameter of a single strand is predicted to be 23 Å, while that of the fiber is 46 Å. These theoretical dimensions are in good agreement with those determined with electron microscopy. The 30 s species, if modeled as a cylinder, consists of 4-5000 23 by 86 Å monomers (46) and would have a molecular weight of approximately 75 million.

The trypsin-mediated (26) polymerization of coagulin

illustrated in Figure 3 follows a sigmoidal curve. The reaction begins slowly and then accelerates in a fashion that implies the cooperative association of particles. These two reaction rates are characteristic of a two-stage nucleated polymerization reaction which can result in helical fibers (16). However, in the coagulin polymerization process, the final result is a gel. At pH 2.5, there are 30 s particles present in solution, but these solutions do not significantly scatter light at 320 nm. Therefore, the turbidity increase measured in Figure 3 probably is not due to fiber growth. It is more likely the result of gel formation. The lag phase in the first two minutes may be fiber formation, perhaps the formation of the 30 s particles. This would then be followed by the faster phase, the lateral association of the fibers into the three-dimensional turbid gel.

Effect of pH

Initial experiments in the search for stable intermediates were based on the reversible depolymerization of the coagulin gel (26). Acid titration of the gel results in the sigmoidal shape of a curve with an apparent midpoint of pH 5 to 5.5 (Figure 4). This suggests that the removal and addition of protons to coagulin plays an important role in the stability of the gel. However, even though low pH destabilizes the three-dimensional coagulin gel, a 30 s

species remains intact at pH 2.5. The protons, therefore, may be titrating groups involved in the lateral association of the coagulin fibers, presumably the 30 s particles. Side chain carboxyl groups in some proteins have been found to have intrinsic dissociation constants, pK_{int} , of 4.7 (47). It is possible that the addition of protons to one or more aspartate and glutamate residues near the surface of the coagulin fibers may, directly or indirectly, disrupt fiber-fiber interactions.

Effect of Temperature

Figure 9 illustrates that a slow rise in temperature does not affect the turbidity of a partially dissolved coagulin solution. The temperature increase did not favor gel formation or polymer dissociation. This suggests that the enthalpy change for gel formation is small. Therefore, entropy is probably the major contributor to repolymerization. The enthalpy change for deprotonation of a carboxylic hydrogen is small while the negative change of entropy associated with its titration is large. In contrast, imidazole and histidine proton titrations involve large enthalpy and small entropy changes (48). This supports the idea that a carboxyl group may play a role in gel formation and stability. In the coagulin gel network, deprotonated side chain carboxyl groups near the outer surface of the fibers could be involved in salt bridges or as acceptors in hydrogen bond formation between the fibers. Alternately, protonation could cause a conformational

change that masks the contact site needed for association.

Effect of Pressure

In accordance with the LeChatelier principle, when pressure is applied to a system, the system will adjust so as to return to a state of equilibrium. In the polymerization of I_p coagulin, several, perhaps conflicting, pressure-induced phenomena are observed. At pH 4.6 and with an initial coagulogen concentration of 810 µg/ml, pressure appears to trigger gel formation. With the pH slightly more acidic (pH 4.4) and with a lower initial coagulogen concentration (421 µg/ml), a gel does not form with an applied pressure. In fact, depolymerization seems to be occurring. Even with the pressure from the gravitational field at 36,000 or 56,000 rpm, a coagulin solution at pH 2.5 can not polymerize to the gel or the 3800 s species. A 30 s fiber is stable, perhaps due to the protonation of the sites which may play a role in the lateral association of fibers that leads to gel formation. Fiber-fiber interactions can not compete with the numerable fiber-proton interactions, so larger forms are not favorable. Therefore, only at pHs near the apparent titration midpoint is there an observed pressure effect on the coagulin polymerization system.

When pressure is applied to a system, the solution adjusts towards the form with the smaller volume. Many biochemical polymers depolymerize with increased pressure

(34). In these systems, reducing the degree of polymerization, and therefore increasing the solvent-particle interactions, results in the solution having a smaller volume. My data (Figures 7) shows that increased pressure causes coagulin assembly into a gel (i.e. phase separation occurs). Apparently, phase separation leads to a solution with a smaller volume.

The data in Figure 7 is consistent with gel formation (i.e. phase separation) rather than simple aggregation of coagulin monomers. The boundary formed in a coagulin solution at pH 4.6 migrated as if the species sedimenting was a gel (44). The repolymerization of the coagulin gel apparently was triggered by the pressure created by the gravitational field. When a gel is subjected to centrifugal force, the partial hydrostatic pressure at the base of the cell causes the gel at that position to collapse. However, the partial pressure at the air/liquid meniscus is lower than the swelling pressure (the pressure associated with imbibition), so the gel here absorbs the solvent released from the collapsed gel. Therefore, it appears that no sedimentation is occurring. This explains why in Figure 5, at 10,000 rpm (triangles) there is no apparent boundary, yet there is light scattering across the sector which increases from the meniscus to the cell bottom. A gel is present. Increasing the rotor speed to 20,000 rpm gives the partial pressure at the bottom of the cell the advantage over the swelling pressure at the top. The

gel now completely collapses and sediments. According to Svedberg and Pedersen the apparent sedimentation coefficient of the gel will decrease until the gel approaches equilibrium where the two pressures (the hydrostatic and swelling pressures) are equal at all positions in the sector (44). It is readily apparent from Figure 7 that the sedimentation velocity of the boundary decreased with time.

These observations can be rationalized in terms of solution volume change, if we recall the effects of pH and temperature on the system. As implied by the titration and temperature data (Figures 4 and 9, respectively) the addition and removal of carboxyl protons may be important in gel formation. The titration of carboxyl protons is entropically driven and is accompanied by a negative volume change due to electrostriction (48). Increasing pressure on a solution containing protonated carboxyl groups will cause them to deprotonate. Water molecules will orient their dipoles around the newly formed charges. At the same time, the deprotonated coagulin particles can now reassociate into the gel. All together this process must result in a negative volume change. The pressure created by the gravitational field apparently has caused the phase transition between coagulin particles in solution and the coagulin gel.

In contrast to this, the cyclooctane layering experiment (Figure 8) appears to show a pressure induced depolymerization. This suggests that a solution of coagulin aggregates

smaller than 3800 s has a smaller volume than the coagulin gel. To have a negative volume change, the system must move toward the monomeric form. Perhaps in order to get a smaller molar volume, this size of polymer must depolymerize. Therefore, the apparent ambiguity in my results could be due to the coagulin polymers tending toward a common, middle, stable size.

Resolving the polymerization and depolymerization effects of pressure is difficult. At least some large forms of the gel have smaller molar volumes than other polymeric forms. Figure 7 shows the gel sedimenting during the course of the run as if it had an apparent sedimentation coefficient around 300 s. This form, apparently a gel, appears to be stable at this pressure. However, at 3800 s (Figure 8) the system has reached a point where increased pressure induces depolymerization. Given all the problems inherent in interpreting the sedimentation velocity data, other methods should be chosen to continue the study of the pressure effect. It is difficult to determine sedimentation coefficients or molecular weights from systems that are pelleting and/or depolymerizing. Although its density and solubility should have kept it from entering the coagulin solution, cyclooctane may not be a passive component of the experiment. Studying the effects of pressure on the optical properties of this protein will help us gain a better understanding of the mechanism of the Lp coagulin polymerization reaction.

Summary

Gelation in the horseshoe crab, *Limulus polyphemus*, appears to be a two-stage process. The data presented here suggest that the initial phase involves coagulin association into a fiber, perhaps the 30 s particle. Complete gelation occurs during the second phase when coagulin fibers laterally aggregate. Evidence from temperature, pH, and pressure experiments suggest that carboxyl protons, directly or indirectly, play a role in gel formation and stability. The net result of coagulin polymerization is a wound-sealing gel (a clot) in the injured tissue.

PART II

Purification and Partial Characterization of a Novel Trypsin
Inhibitor from the Hemolymph of the Horseshoe Crab *Limulus*
polyphemus

INTRODUCTION

Proteinase inhibitors play a significant role in the regulation of proteolysis, whether the target enzymes are of exogenous or endogenous origin. Some protein inhibitors, like antithrombin III, inactivate their target enzyme by binding to its active site (49). Other inhibitors alter reactions by engulfing the enzyme, thus removing it from the environment (50). Regardless of the mechanism of action, proteinase inhibitors permit regulation of the extent and rate of proteolysis in the presence of active proteinases. Protein inhibitors of mammalian serine proteinases have been identified from numerous sources, including soybean (51), human pancreas (52), and tobacco hornworm (*Manduca sexta*) larvae hemolymph (53).

Proteinase inhibitors of both cellular and plasma origin have been described from Lp. The cellular proteinase inhibitors include an acid- and heat-stable factor (molecular weight of 6100) which is active against trypsin, chymotrypsin and thermolysin, a small amount of an α_2 -macroglobulin homologue (54), and an acid labile factor which is effective against the final proteinase in the Lp coagulation pathway (55). The Lp α_2 -macroglobulin homologue is the only proteinase inhibitor reported to be in the plasma (55).

I have recently discovered a potent trypsin inhibitor

copurifying with preparations of Lp coagulogen. This proteinase inhibitor is distinct from those already described from Lp and appears to be structurally different from other known trypsin inhibitors. Here I report the isolation and partial characterization of this proteinase inhibitor from the hemolymph of Lp.

MATERIALS

In addition to those materials listed in Part I, Materials, paragraph one, the following were required to perform the experiments in this part of the dissertation. Basic fuchsin was obtained from Kodak. Ninhydrin was from Beckman. Kimble screw cap vials with silicone septa and constant boiling, sequanal grade 6 N HCl and norleucine from Pierce were used in the amino acid analysis. Cysteine, trypsin, papain, pepsin, protease X (thermolysin), chymotrypsin, N α -Benzoyl-DL-arginine *p*-nitroanilide (BAPNA), and casein were procured from Sigma. All reagent grade solution components were supplied by Baker.

METHODS

Protein Preparation

Limulus trypsin inhibitor (LTI) was isolated from horseshoe crab hemolymph via a modification of the procedure of Shishikura *et al* (24) to purify coagulogen (Appendix A). LTI was separated from coagulogen by passage through a carboxymethyl-Sephadex column (1.2 x 16.2 cm) equilibrated with 0.1 M ammonium bicarbonate, pH 8.1. 1.0 M ammonium bicarbonate, pH 8.1 was then added to elute proteins bound to the column. The peak fractions were pooled and concentrated using a Millipore CX-10 ultrafiltration unit. Purity was assessed by 10% SDS-PAGE (25). Approximately 1 mg of LTI was isolated from 100 ml of acidified hemolymph.

Clotting Assays

The polymerization or clotting of coagulogen can be triggered *in vitro* with trypsin (26). The clotting assays were performed as described by Nakamura *et al* (27). Each assay tube contained 1 ml of 50 mM Tris-HCl buffer, pH 8.0 and 0.5 ml of coagulogen (approximately 0.7 mg/ml). The reaction was initiated with the addition of 0.02 ml of varying concentrations (0.1 to 1.0 mg/ml) of trypsin in 0.001 N HCl. The time course of the clotting reaction was monitored by the absorbance change at 320 nm. The spectrophotometer was

zeroed at 320 nm with the coagulogen/Tris-HCl solution before the addition of trypsin.

Protein Determination

Protein content was estimated using the absorbance at 280 nm assuming an extinction coefficient of 1 mg/ml·cm. Absorbance profiles of LTI between 180 and 300 nm were determined with a Perkin Elmer (Coleman 124) double beam spectrophotometer. A fluorescence profile of LTI at various excitation and emission wavelengths was produced using a Farrand Optical Co., Inc. spectrofluorometer (Mark I).

Amino Acid Analysis of LTI

Samples of LTI in 1.0 M ammonium bicarbonate, pH 8.1 were lyophilized, dissolved in deionized water and relyophilized to remove any residual buffer. 1 ml of 6 N HCl and an internal standard were added to each vial. After a 10 min nitrogen purge, the vials were sealed and the samples hydrolyzed for 24 h at 110 °C. After drying *in vacuo* the amino acid content was analyzed by a Beckman Model 118CL amino acid analyzer (56).

Amino-terminal Amino Acid Sequence of LTI

Samples were prepared for solid phase sequencing by first dialyzing LTI (approximately 230 µg) with 0.1 M sodium carbonate, pH 9.95 to remove ammonia from the sample. Disulfide bonds were reduced with tributyl-phosphine (57).

Approximately 1 nmol of a sample was covalently attached to a diisothiocyanate Sequelon membrane and sequenced with a 6600 Milligen/Biosearch proSequencer.

Another aliquot of purified LTI (containing 200 μ g of protein) was dialyzed with 10% (vol/vol) acetic acid. The sample was then lyophilized to remove the acetic acid. A duplicate partial amino-terminal sequence was determined with an Applied Biosystems, Inc. 470A sequenator equipped with on-line phenylthiohydantoin-analysis.

Sedimentation Equilibrium

Sedimentation equilibrium experiments were conducted with a Beckman Model E analytical ultracentrifuge equipped with a temperature control, Rayleigh interference optics, an electronic speed control, and a 20 mW helium-neon laser light source (28). The temperature of the AN-D rotor was regulated at 23.3 °C. Analyses at 40,000 and 48,000 rpm were performed using a six-channel, 12-mm-thick, charcoal-filled epon centerpiece and sapphire windows.

LTI (approximate concentration 0.308 mg/ml) was dialyzed with stirring against three changes of 0.1 M ammonium bicarbonate (1:1000 vol:vol) at 4 °C for 28 h. The sample was centrifuged for 5 min following dialysis and dilutions were made using the final dialysate.

High speed equilibrium experiments and blanks were carried out as described by Yphantis (29). Three sets of four

interferogram exposure series were made at 30 min intervals after the estimated equilibrium time (29) had elapsed for each speed. Fringe displacement data for each of five fringes were obtained from the interferograms at a radial spacing (in cell coordinates) of 9 μm from the meniscus to the bottom of the cell using an automated photographic plate reader (58,59). Data were edited using REEDIT (kindly provided by David Yphantis). The reduced molecular weight (30) was estimated using nonlinear least squares analysis, NONLIN (31).

Proteinase Assays

The inhibition by LTI of trypsin-catalyzed hydrolysis of BAPNA was determined using a modification of a previously described procedure (53). The standard assay mixture contained 50 μl of 0.1 M Tris-HCl, pH 8.0 containing 0.01 M CaCl_2 , 50 μl of 0.05 mg/ml of trypsin (2.2 μM , final concentration 6.5 $\mu\text{g}/\text{ml}$) in 0.001 N HCl and either 50 μl of LTI (7.9 μM) or 50 μl of buffer. Blank tubes contained deionized water instead of enzyme. The reaction was initiated with the addition of 100 μl of BAPNA (0.25 mM to 1.0 mM) in the buffer. After 30 min at 37 $^\circ\text{C}$ the reaction was stopped with 0.5 ml of 30% vol/vol acetic acid. The percentage of inhibition (%I) was calculated as:

$$\%I = [1 - (A_1/A_0)] \times 100 \quad \text{Equation 10}$$

where A_1 and A_0 are the absorbances with and without inhibitor, respectively (53). The appearance of the *p*-nitroanilide

product was monitored spectrophotometrically at 410 nm.

The inhibitory activity of LTI on the digestion of casein by trypsin and other proteinases was examined using an assay mixture that included 50 μ l of buffer, 50 μ l of 0.05 mg/ml enzyme, 50 μ l of LTI (0.13 mg/ml, 7.9 μ M) or buffer (the latter serving as control). Upon the addition of 100 μ l of 0.17% (weight/vol) casein solution in 0.1 M Tris-HCl, pH 8.0, the tubes were incubated at 37 °C for 20-30 min. The reaction was terminated with 0.5 ml of 5% trichloroacetic acid and the tubes were allowed to stand at room temperature for 1 h. The precipitate was removed by centrifugation and the absorbance at 280 nm was measured (60). The percent inhibition was calculated with equation 10. The enzymes and their respective buffers are as follows: chymotrypsin or trypsin in 0.001 N HCl added to 0.1 M Tris-HCl, pH 8.0; thermolysin in 0.1 M Tris-HCl with 0.01 M CaCl₂, pH 8.0 added to the same buffer for the assay; papain in deionized water added to 0.1 M Tris-HCl, pH 8.0 (with 50 μ l of 1 mM cysteine with 0.02 M EDTA, pH 8.4 added subsequently to activate the papain); and pepsin in 0.01 M sodium acetate, pH 5.4 added to the same buffer for the assay.

The effect of LTI on the mammalian blood clotting protein thrombin was assayed using 300 μ l of 0.1 mM Spectrozyme TH as the substrate, 50 μ l of 1 M ammonium bicarbonate (blank tube) or 50 μ l of LTI (0.2 mg/ml) (inhibition tube), and 13.5 μ l of deionized water (control) or 13.5 μ l of thrombin (equalling

1 NIH activity unit). LTI and thrombin were mixed and allowed to incubate for 1 to 2 min before the addition of substrate. Reactions were monitored spectrophotometrically at 405 nm for 3 min.

To determine its activity on blood coagulation in Limulus, 200 μ g of LTI were sent to Cape Cod Associates, Woods Hole, MA. Experiments were conducted with the Limulus amoebocyte lysate (LAL) assay (the assay used to detect endotoxin in intravenous fluids (4)) to determine the endotoxin-binding activity of LTI. Serial dilutions of LTI were made (down to 8 μ g) and each sample was incubated with 1 μ g/ml of Gram-negative endotoxin in a microtiter plate. After addition of the LAL reagent, any neutralization of the endotoxin effect on the reagent by LTI was determined (personal communication from Dr. Norman Wainwright).

RESULTS

Identification of an Inhibitor of Coagulogen Polymerization

It has been previously shown that the serine proteinase trypsin can catalyze the polymerization of purified coagulogen preparations (26,27). Efforts to examine this polymerization phenomenon were hampered initially by the presence of a small quantity of a clotting inhibitor which co-eluted with coagulogen in the preparation. It will be demonstrated that this protein is a potent trypsin inhibitor.

In initial studies, coagulogen was prepared by column chromatography with Sephadex G-50. A typical chromatographic elution profile is shown in Figure 10. Clottable protein eluted in the second and major chromatographic peak of the Sephadex G-50 column. Clotting assays were performed on two different preparations of coagulogen using two different concentrations of trypsin. It was observed that one preparation gelled in the presence of low concentrations of trypsin (0.1 mg/ml), while a second preparation of coagulogen required a higher trypsin concentration (0.5 mg/ml) to induce polymerization (Figure 11). The addition of aliquots from the other three G-50 column eluted peaks had no inhibitory effect on the polymerization reaction (Figure 12). These results could be explained by the presence of an inhibitory factor affecting the clotting reaction.

Figure 10:

Elution profile of acid-treated Lp hemolymph from a Sephadex G-50 column, equilibrated with 0.1 M ammonium bicarbonate, pH 8.1. Purification protocol is described, in full, in Appendix A. Approximately 2.5 ml were collected per fraction at a rate of 40-50 ml per h. Coagulogen elutes in peak II.

Figure 11:

Trypsin-catalyzed polymerization of two different Lp coagulogen preparations. Each assay contained 1.0 ml of 50 mM Tris-HCl, pH 8.1, 0.5 ml coagulogen and 0.02 ml of trypsin in 0.001 N HCl. Change in turbidity with time was monitored at 320 nm. The absorbance (A) values for the two assays from each coagulogen preparation were normalized (A_{320}/A_{320max} , where A_{320max} is the final, stable absorbance at 320 nm). Preparation I (0.7 mg/ml) with open circles 0.5 mg/ml trypsin (final concentration 6.5 μ g/ml) or closed circles 0.1 mg/ml trypsin (1.3 μ g/ml); Preparation II (1.6 mg/ml) with open triangles 0.5 mg/ml trypsin or closed triangles 0.1 mg/ml trypsin.

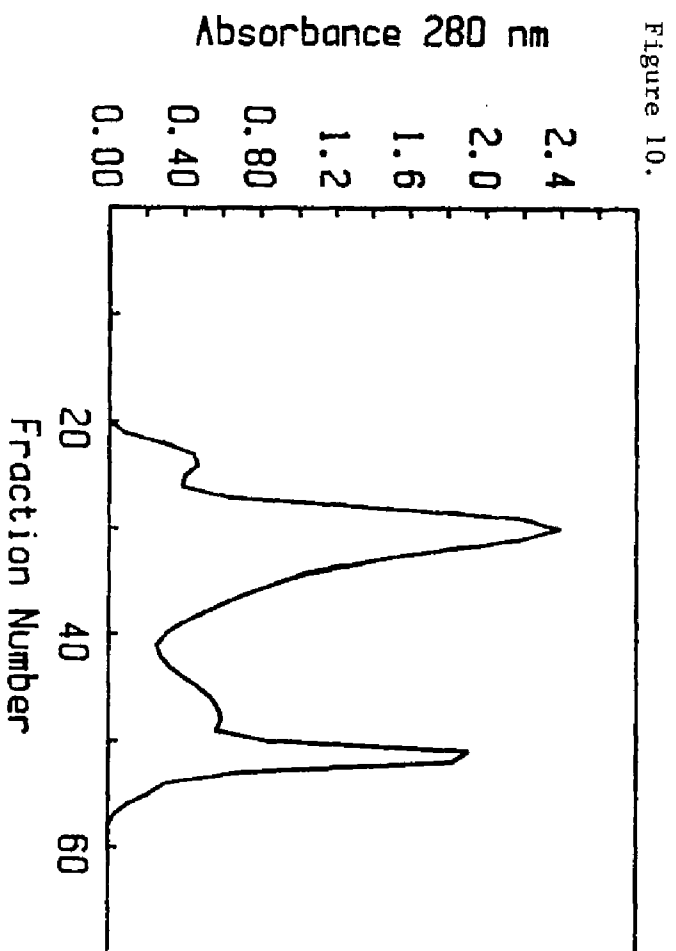


Figure 11.

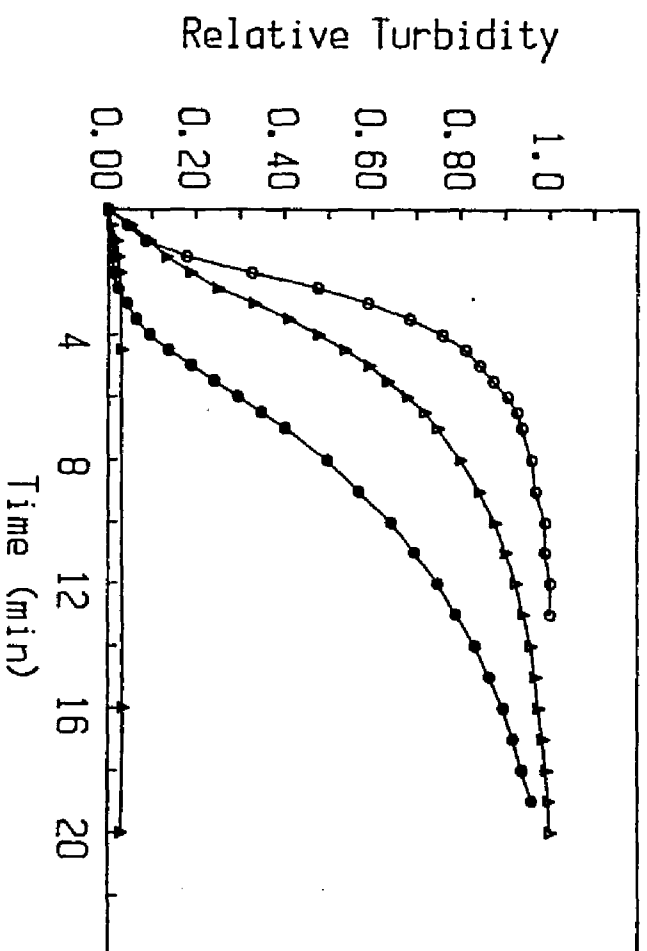


Figure 12:

Addition of aliquots of the unclottable G-50 Sephadex elution peaks had no effect on the polymerization reaction. Each assay included 1.0 ml of 50 mM Tris-HCl, pH 8.1, 0.5 ml of Preparation II coagulogen (1.6 mg/ml) and 0.02 ml of 0.5 mg/ml trypsin (final concentration 6.5 μ g/ml). Closed circles are a typical clotting assay; open circles are an assay with 10 μ l of peak I (optical density (O.D.₂₈₀) = 0.464); squares are an assay with 9 μ l of peak III (O.D. = 0.454); and triangles are an assay with 3 μ l of peak IV (O.D. = 1.799).

Figure 13:

The effects of the removal of LTI from coagulogen on the trypsin-mediated polymerization reaction. Each assay contained 1.0 ml of 50 mM Tris-HCl, pH 8.1, 0.5 ml coagulogen (0.9 mg/ml) and 0.02 ml of 0.1 mg/ml trypsin (87 pmol, final concentration 1.3 μ g/ml) in 0.001 N HCl. Open circles are an assay of coagulogen before removal of LTI; closed circles, polymerization of coagulogen after removal of LTI with the carboxymethyl-Sephadex column; open triangles, addition of 0.02 ml of LTI (123 pmol) to assay; closed triangles, addition of 0.02 ml of a 1:2 (vol:vol) dilution of LTI to assay.

Figure 12.

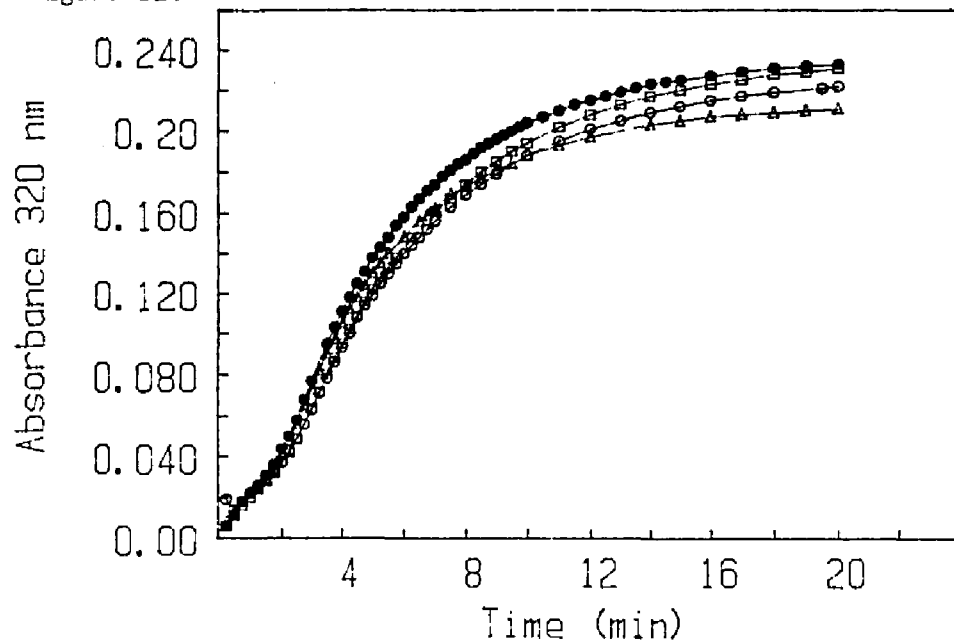
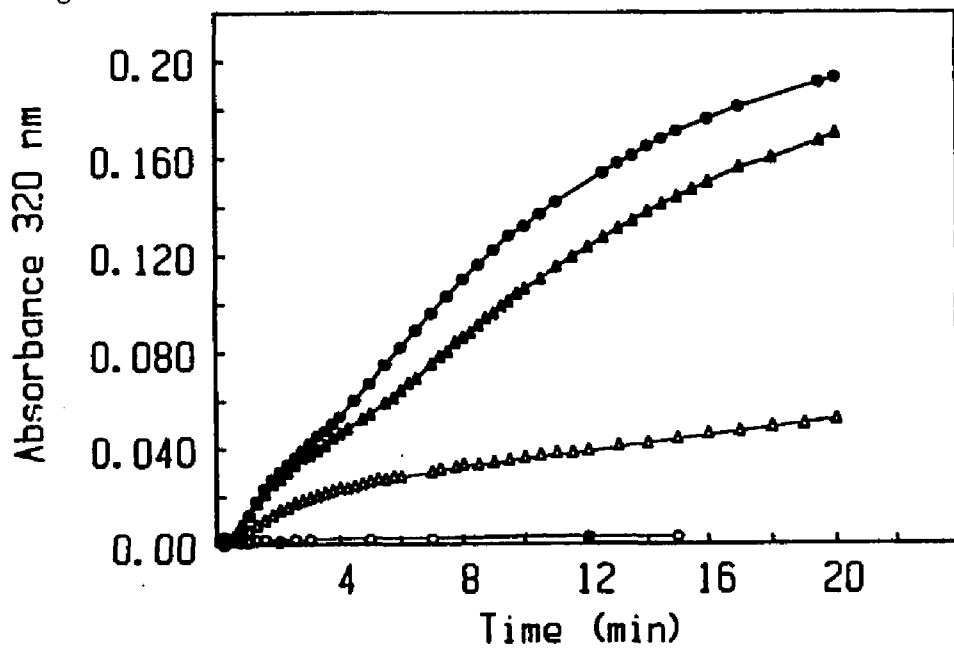


Figure 13.



Isolation of the Inhibitory Factor

In an effort to identify the nature of the inhibition of coagulogen polymerization, the coagulogen preparation was fractionated by passage through a carboxymethyl-Sephadex column pre-equilibrated with 0.1 M ammonium bicarbonate buffer. Coagulogen was not retained by the column under these conditions; this coagulogen preparation now could be polymerized with the addition of 87 pmol trypsin (Figure 13, filled circles). Increasing the ionic strength of the elution buffer to 1.0 M caused the elution of a single peak from the carboxymethyl-Sephadex column. Addition of aliquots of this material to the clotting assay resulted in inhibition of the clotting reaction in a concentration dependent manner (Figure 13, open and filled triangles). Two inhibited clotting assay solutions, each containing enough trypsin (87 pmol) to clot inhibitor-free coagulogen, were allowed to stand overnight. One assay solution consisted of LTI-containing coagulogen; the other solution had inhibitor-free coagulogen mixed with a 6-fold molar (555 pmol) excess of LTI. Even with the extended time, neither assay solution clotted. This result suggests that the inhibitor/enzyme interaction is strong and essentially irreversible.

Initial Characterization of LTI

Purified LTI ran as a doublet on SDS-PAGE under both reducing and nonreducing conditions (Figure 14). In the

Figure 14:

SDS-PAGE of LTI eluted from the carboxymethyl-Sephadex column. Samples of LTI (8.6 μg), with and without 2% β -mercaptoethanol, were loaded on a 10% SDS-PAGE gel (25). After electrophoresis, the protein bands were visualized with Coomassie Brilliant Blue staining.

Lane 1: M_r standards (1 μg of each protein loaded)

Lane 2: LTI run under nonreducing conditions

Lane 3: LTI run under reducing conditions

kD

1

2

3

97.4

66.2

42.7

31.0

21.5

14.4



presence of reducing agent LTI migrated as a species with an apparent molecular weight of 15,000. The molecular weight estimate for LTI under nonreducing conditions is 20,000. No reducing carbohydrate was detected when a 10% SDS-PAGE gel (25), loaded with 5 μ g of protein, was stained with Schiff reagent using the modified procedure described by Fairbanks *et al* (61). However, given the sensitivity of the staining procedure (62) it can only be stated that LTI is less than 40%, by mass, carbohydrate.

LTI has a UV absorbance maximum between 278 and 279 nm. Although there is no apparent shoulder at 295 in the absorbance profile, excitation of LTI at 295 nm produces a fluorescence peak at 340 nm suggesting the presence of tryptophan residue(s) in LTI (data not shown).

Amino Acid Content

The amino acid composition of LTI is shown in Table 1. The values for the number of residues per molecule of LTI are the averages of three data sets, assuming a molecular weight of 16,300 (from sedimentation equilibrium). Two data sets are duplicate determinations of the same LTI preparation; the third set is from a second inhibitor sample. Tryptophan content was not determined. Note that asparagine and glutamine are hydrolyzed to their acid forms and analyzed as such. The molecular weight calculated from this composition is 15,476. The partial specific volume of LTI, based on the

Table 1. Amino Acid Composition of LTI

Amino Acid	LTI ^a	Std. Dev. ^b
Asp/Asn	11.2	0.9
Thr	7.4	0.4
Ser	9.6	0.6
Glu/Gln	12.1	1.0
Pro	10.7	0.7
Gly	13.0	0.4
Ala	9.2	0.9
Cys	5.2	1.0
Val	9.3	1.1
Met	0	---
Ile	5.8	0.6
Leu	8.7	0.4
Tyr	7.1	0.7
Phe	5.1	0.4
His	4.1	0.7
Lys	11.5	0.3
Arg	10.1	0.9
Trp	n.d. ^c	---
Total	140.1	

^a The units are residues per molecule. The values are averages of three data sets of ratios of the residues and were calculated based on the molecular weight of 16,300.

^b Standard deviation values calculated for each amino acid from three data sets.

^c Tryptophan composition was not determined.

amino acid composition is 0.71, ml/g (39).

The amino acid composition of LTI was compared to the composition of trypsin inhibitors listed in the NBRF database (63), using the method of Cornish-Bowden (64). None of those with comparable lengths showed any degree of relatedness to LTI.

Amino-terminal Amino Acid Sequence

The sequence of the amino-terminal twenty amino acids of LTI is:

1	10
Val-Ser-Pro-Pro-Phe-Ile-Lys-Gln-Thr-Lys-	
Phe-Ser-Thr- X -Phe-Leu-Gly- X -Ser-Ser.	

The initial yield was 25%, based on the recovery in the first sequencing cycle (typical for the methods employed). Only a single species was detected at the amino-terminal end (Val). This suggests that the doublet seen on the SDS-PAGE gel (Figure 14) may be indicative of two forms of LTI. Perhaps a blocking group is attached to one of the two ends of LTI in some of the sample and, therefore, causing altered mobility on the gel. In the solid phase sequencing method used, cysteine residues are destroyed and thus are not detectable. Since no amino acid was observed during cycle 14 (of both analyses), it is possible that residue 14 is cysteine. The techniques used could not precisely identify residue 18.

This sequence was compared to amino acid sequences in the

NBRF protein sequence database, using the IALIGN and FASTA programs (63). There were no apparent similarities between the amino-terminal sequence of LTI and any sequence in the database, including a number of known trypsin inhibitors and Lp coagulogen.

Sedimentation Equilibrium Analysis

Under reducing conditions, LTI migrated farther than it did in the absence of β -mercaptoethanol (Figure 14). Since this is the reverse of what is usually seen, it is necessary to use another technique to ascertain the molecular weight of LTI. Sedimentation equilibrium in the analytical ultracentrifuge is a primary technique for determining the molecular weight of a macromolecule. The sedimentation equilibrium data from two solution samples and at two rotor speeds (40,000 and 48,000 rpm) were analyzed simultaneously to estimate the reduced molecular weight, σ (30). The data fit to a model consisting of a single ideal thermodynamic component (the root mean square of the variance of the fit was 6.2 μm). Using σ and the \bar{v} calculated from the amino acid composition, the molecular weight of LTI is calculated to be $16,300 \pm 700$ (the 65% confidence interval values returned by NONLIN were symmetrical and thus correspond to standard deviation). The samples were homogenous, as judged by this technique, suggesting that the doublet observed by SDS-PAGE is not reflected in the native structure (29).

Specificity of LTI

The inhibitory effect of LTI on the hydrolytic activity of the serine proteinase trypsin was examined. LTI caused almost complete inhibition of the trypsin-catalyzed hydrolysis of casein, a high molecular weight substrate (Table 2). Trypsin (2.2 μ M) activity on various concentrations (0.25 mM to 5.0 mM) of a low molecular weight substrate, BAPNA, also was inhibited almost completely (average percent inhibition 94%) by LTI (7.9 μ M). The proteinase specificity of LTI was studied using proteinases with different active site residues and casein as the substrate (Table 2). LTI was effective in inhibiting the action of the serine proteinase chymotrypsin. The inhibitor shows no significant effect on papain (a thiol proteinase), thermolysin (a zinc metalloproteinase), pepsin (an aspartyl proteinase), or thrombin (a serine proteinase) (data not shown). The ability of LTI to inhibit the hydrolysis of BAPNA indicates that it is an active site inhibitor.

In an attempt to determine a possible role for LTI in the Limulus blood coagulation system, LTI was incubated with endotoxin and mixed with the Limulus amoebocyte lysate (LAL) reagent. At 50 μ g/ml and below, there was no inhibition of the LAL reagent by LTI. At higher concentrations (200:1 molar binding ratio of LTI to endotoxin) only a slight neutralization of the endotoxin-mediated triggering of the gelation was seen (personal communication from Dr. Norman Wainwright).

Table 2. Effect of LTI (7.9 μ M) on Different Proteolytic Enzymes Using Casein (62 μ M) as Substrate

enzyme	n ^a	mean %I ^b	LTI/enzyme ^d
trypsin	3	94.1 \pm 3 ^c	3.7
chymotrypsin	2	97.0	4
pepsin	2	0	6
thermolysin	2	3.2	5.4
papain	2	2.6	3.7

^a number of assays

^b percent inhibition, %I, equation is stated in methods
Assays were monitored at 280nm.

^c value indicates standard deviation

^d mole ratio of LTI to enzyme

The LAL reagent is composed of the endogenous Limulus clotting factors. The failure of LTI to inhibit the gelation of the reagent suggests that it has no apparent role in Limulus blood coagulation.

DISCUSSION

Proteinase inhibitors have been identified previously in the hemolymph of *Limulus polyphemus* (Lp) (54,55), but only the α_2 -macroglobulin homologue has been purified to date (65). Here the isolation, characterization and partial amino acid sequence of a novel trypsin inhibitor from Lp hemolymph is described. When compared to previously reported Lp inhibitors it is clear that LTI is a distinct protein. The molecular weight of LTI is 16,300. LTI is able to inhibit the hydrolysis of both high and low molecular weight substrates by trypsin, the latter suggesting that LTI affects the active site of the enzyme. This inhibitor also inhibits the activity of chymotrypsin. By virtue of its stability in acid during the isolation procedure and its inability to inhibit the Lp coagulation cascade, LTI is not the acid-labile factor reported by Armstrong *et al* that does inhibit the Lp clotting enzyme (55). With a subunit molecular weight of 180,000-185,000 and an inability to inhibit the hydrolysis of low molecular weight substrates, the α_2 -macroglobulin homologue of Lp is clearly distinct from LTI (65). The acid-stable inhibitor from Lp is also not LTI because of its lower molecular weight (6100) and its ability to inhibit thermolysin (54).

Protein inhibitors of enzymatic activity are present in

all types of organisms. Proteinase inhibitors that share target enzymes often have sequence similarities in their functional domains. For example, the inhibitory site in the Western sand viper venom basic protease inhibitor I (a trypsin inhibitor) is lysine 17 (66). In the porcine pancreatic secretory trypsin inhibitor, this site is lysine 18 (67). There appears to be a common theme for plant protein inhibitors of proteolytic enzymes. In legume seeds, proteinase inhibitors fall into one of two classes according to their molecular weight and cysteine content. Kunitz type inhibitors have a higher molecular weight (20,000) and four cysteine residues, while a Bowman-Birk type inhibitor is smaller (8000) and more highly crosslinked with disulfide bonds (14 cysteine residues per macromolecule) (68). Recently two trypsin inhibitors were purified and partially sequenced from *Manduca sexta* larvae hemolymph (53). The amino acid sequences of these inhibitors are similar to those of bovine colostrum trypsin inhibitor (69) and Russell's viper venom basic protease inhibitor II (70), indicating that some structural and functional similarities in proteinase inhibitors are common across phyla. Indeed, amino terminal sequences, specificities and physical characteristics of proteinase inhibitors have been described from a wide variety of organisms and tissues (63). Although LTI has a similar function, its molecular weight and amino-terminal sequence suggest that its structure differs from these previously

reported trypsin inhibitors. Thus, the Lp hemolymph trypsin inhibitor described in this part of the dissertation seems to have characteristics that are distinct from all known proteinase inhibitors.

LTI does not appear to play a direct role in the regulation of Lp coagulation. However, proteinase inhibitors are invaluable regulators of proteolysis. Although the physiological role and location of LTI are not known, it probably acts to control the enzymatic activity of trypsin-like serine proteinases.

APPENDIX A

Coagulogen Preparation Protocol

Before bleeding, the fleshy joint between the carapace and abdomen are washed with an ethanol soaked Q-tip. In order to bleed the horseshoe crab the carapace and abdomen shells must be positioned at an acute angle (relative to one another). "Tickling" the legs of the animal sometimes helps get the crab in this position. This position is useful for cleaning the joint, too. Keep the abdomen towards you and almost perpendicular to the floor when cleaning or bleeding.

The basic procedure used is that described by Shishikura *et al* (24). Using a 30 cc syringe containing approximately 5 ml of glacial acetic acid and an 18 gauge needle, carefully insert the needle into the joint about 10 to 20 mm. This should position the needle in the tubular heart. Try to keep the horseshoe crab tilted upward and keep the needle/syringe planar to the carapace. Gently pull on the plunger to remove hemolymph from the animal. If this is difficult and no blood is flowing, pull the needle out a little. If the needle is in too far, it will have entered the body cavity. The needle can be removed and reinserted. Do not get any of the acetic acid on or in the animal.

As the blood (bluish) reacts with the acetic acid, it

becomes white and clumpy. Once the syringe is full, remove it slowly from the animal and shake vigorously to further mix the hemolymph and acetic acid. The final concentration of acetic acid will be about 17% vol/vol. Empty the contents of the syringe into a clean beaker (you may have to remove the plunger and dump the acidified hemolymph out from the back end). Repeat this until all of the horseshoe crabs are bled. All of the hemolymph should be collected in one beaker. If so desired another aliquot of acetic acid can be added to the beaker, as the bleeding is going on, to ensure that all of the hemolymph has been acidified. The acidified hemolymph is allowed to stand at room temperature for 1 h.

After standing, the acidified hemolymph is homogenized with a Polytron until the solution is the consistency a thick milk shake with no lumps. This solution is poured into previously prepared dialysis tubing (71). 75-100 ml of acidified hemolymph is dialyzed against 4 liters of deionized water (the bag must float). The dialysis is done at 4 °C for 18-24 h with two changes of water in that time.

Following dialysis, the precipitate is removed by low speed centrifugation (9500 rpm, 20 min) and the pooled supernatant is concentrated by precipitation with 50% saturated ammonium sulfate. The ammonium sulfate treated solution can sit at room temperature for 2-3 h or at 4 °C overnight. Swirl the flask occasionally.

The coagulogen-containing ammonium sulfate precipitate

is separated from the supernatant (9500 rpm, 20 min). The precipitate is dissolved in 5 to 10 ml of 0.1 M ammonium bicarbonate, pH 8.1. Any flocculant material remaining after dissolution must be removed by centrifugation (9500 rpm, 20 min) prior to chromatography. The coagulogen-containing sample is gel-filtered on a Sephadex G-50 (fine grade) column (1.7 x 120 cm, included volume is approximately 200 ml) equilibrated with 0.1 M ammonium bicarbonate, pH 8.1. Fractions (approximately 2.5 ml per tube) are collected with a flow rate of 40-50 ml per hour (a flow rate of 10-20 ml per hour would minimize axial dispersion but no significant loss in resolution was seen at the higher flow rate). The elution of protein is monitored by the absorbance at 280 nm. Peak fractions are pooled. The coagulogen-containing peak is identified by clot formation of an aliquot with the addition of trypsin. Sample purity is assayed using SDS-polyacrylamide gel electrophoresis (25). Incubation with carboxymethyl- and diethylaminoethyl-Sephadex beads removes other non-clottable proteins from the preparation. As stated in Methods (Parts I and II), a carboxymethyl-Sephadex column is used to separate coagulogen from *Limulus* trypsin inhibitor (LTI). According to Shishikura *et al* (24), 15 to 20 mg of coagulogen can be obtained from 100 ml of hemolymph. The yield from the preparations has varied from 7.5 to 33 mg from 100 ml of hemolymph.

APPENDIX B

Sedimentation Velocity Experiments

Sedimentation velocity experiments will yield information about the size and shape of particles in a solution. The angular acceleration, due to the spinning rotor, in the centrifuge generates the forces necessary to sediment small particles like proteins. The applied force causing the flow, or sedimentation of particles, in the centrifuge is $\omega^2 r$ per unit mass (where ω^2 is the angular frequency, $\omega = 2\pi \text{rpm}/60$). In the absence of diffusion, this force is exactly countered by a frictional force resulting in a constant drift velocity. This velocity will be a function of the size and shape of the sedimenting particle and it will be proportional to the applied force. This proportionality constant is defined as the sedimentation coefficient (s). By finding the s of particles in a solution, estimates of the size and shape of those particles can be made (72).

As the particles sediment in the centrifuge, a layer or pellet forms at the base of the cell. At the other end of the cell, a boundary has formed between the solvent and the solution. During the course of the experiment, more particles leave the solution and enter the pellet. Because of this, the solvent/solute boundary moves. In the analytical ultracentrifuge, it is possible to monitor the movement of this

boundary.

Figure 15 is a basic schematic of an analytical ultracentrifuge (72). The rotor has a hole in it so that light can pass through to a detector. The detector used in the experiments in Part I is a photoelectric scanner. The cell, which contains the sample, sits in the hole in the rotor. The centerpiece in the cell has two sectors or two paths for the light: (1) a reference sector and (2) a sample sector (Figure 16A) (73). Illustrated in Figure 16B is a cross-section of the sample sector (73). The centrifugal force travels from the center of the rotor outward. The boundary, therefore, moves from the air/liquid meniscus to the cell bottom. Using a monochromator lamp set at 280 nm, the detector scans across the sector from cell bottom to meniscus. The output is a tracing of the absorbance.

Figure 17 is a set of voltage tracings from a sedimentation velocity experiment of a coagulin gel at pH 2.5 analyzed at 36,000 rpm. The air/liquid meniscus position (a), the cell bottom (b), and the boundary (c) are marked on the first scan (Figure 17A). The "stair steps" (at the left-hand side of each scan) are in 0.2 optical density units and are used as calibrations for converting the voltage readings to absorbance readings. Examination of this series of scans leads to the following observation. (1) With time, the boundary moves towards the base of the cell (the velocity of this is dependent on the size and shape of the particles).

Figure 15:

The basic elements of sample detection for an analytical ultracentrifuge (72).

Figure 16:

A. A typical double sector cell (73).

B. A cross-sectional view of a sample sector during a particular moment in the experiment. The centrifugal force flows from the center of the rotor out towards the base of the cell (73).

- a. air/liquid meniscus
- b. cell bottom
- c. solvent/solution boundary

Figure 15.

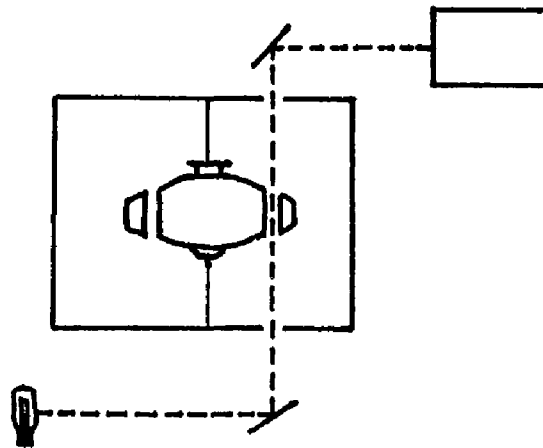
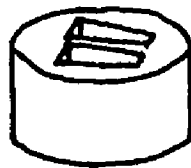


Figure 16.

A.



B.

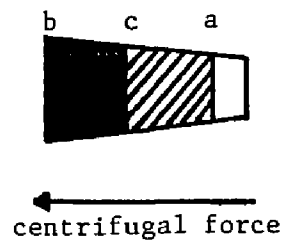
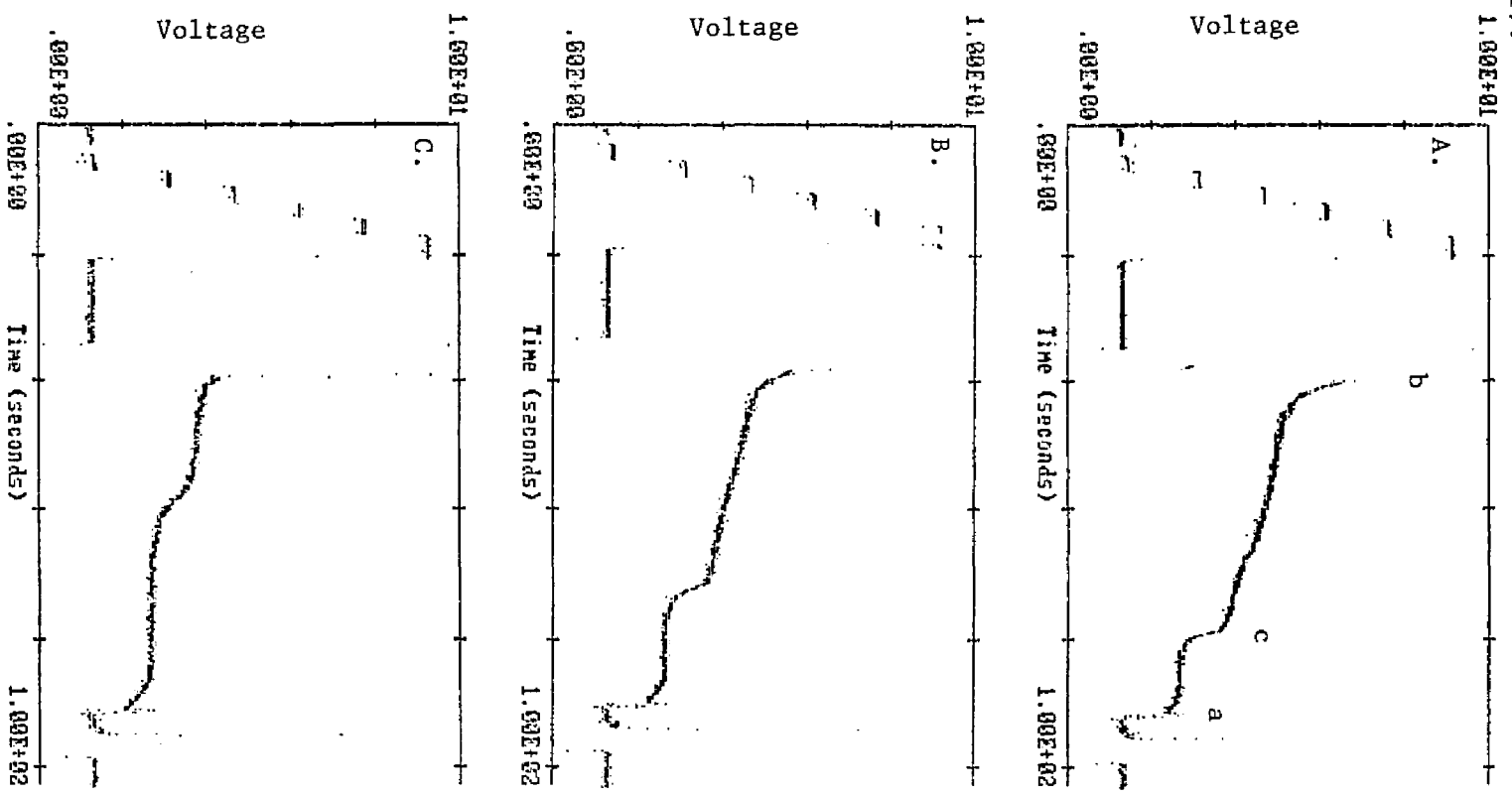


Figure 17:

Absorbance scans (280 nm) of a coagulin solution at pH 2.5 taken at consecutive time points during a sedimentation velocity experiment at 36,000 rpm. The initial coagulogen concentration was 560 $\mu\text{g/ml}$. The time of each scan from zero time (two-thirds final rotor speed (24,000)) is: A: 1192 s, B: 1670 s, C: 3005 s. In A, a is the air/liquid meniscus, b is the cell bottom, and c is the boundary.

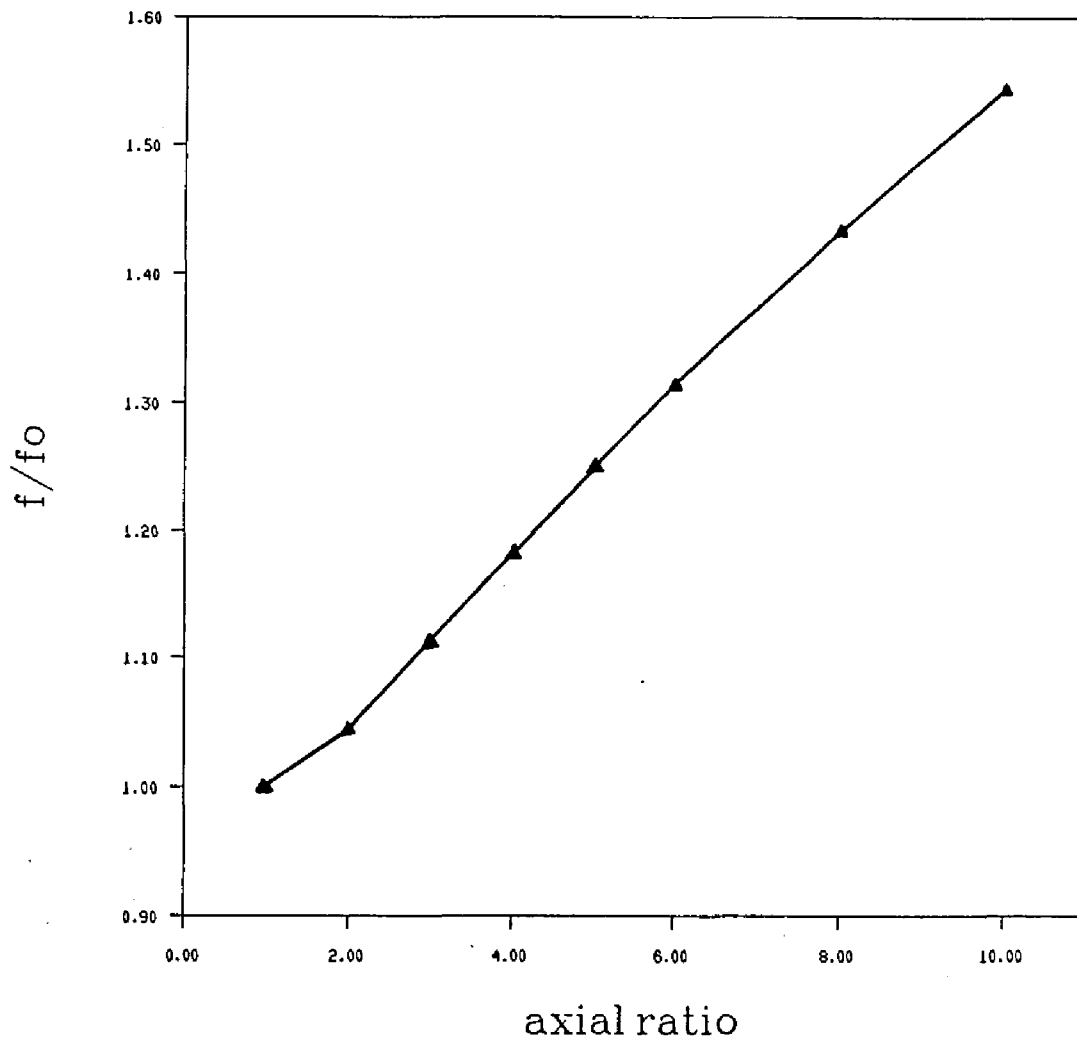
Figure 17.



(2) The concentration at the plateau decreases with time. This phenomenon is due to the radial dilution caused by the shape of the sectors. They are not rectangular, rather, their sides are angled so that the particles travel in a radial path (Figure 16). As the particles travel toward the cell bottom, they enter increasing volumes with each radial slice. In a given slice, the field strength ($\omega^2 r$) is larger at the edge facing the cell bottom. Therefore, particles at this edge are traveling faster and continue to enter larger volumes. As a result of the radial movement of the particles, the plateau concentration decreases. (3) The boundary tends to broaden as a function of time because of diffusion. To understand something about the moving boundary, the scans are converted into a sedimentation coefficient. An explanation of this conversion can be found in Part I, Methods. Such analysis of the scans in Figure 17 can be found in Part I, Results.

APPENDIX C

Figure 18:
A Plot of the Ratio of the Experimental Frictional Coefficient
and the Theoretical Frictional Coefficient (f/f_0) Versus the
Axial Ratio (42)



LIST OF REFERENCES

1. Levin, J. and Bang, F.B. (1964) The Role of Endotoxin in the Extracellular Coagulation of Limulus Blood. Bull. Johns. Hopkins Hosp. **115**, 265-274
2. Zweifach, B.W. and Janoff, A. (1965) Bacterial Endotoxemia. Ann. Rev. Med. **16**, 201-220
3. Levin, J., Poore, T.E., Zauber, N.P. and Oser, R.S. (1970) Detection of Endotoxin in the Blood of Patients with Sepsis due to Gram-negative Bacteria. New Eng. J. Med. **283**, 1313-1316
4. Jorgensen, J.H. and Smith, R.F. (1973) Rapid Detection of Contaminated Intravenous Fluids using the Limulus in vitro Endotoxin Assay. Appl. Microbiol. **26**, 521-524
5. Copeland, D.E. and Levin, J. (1985) The Fine Structure of the Amebocyte in the Blood of Limulus polyphemus. I. Morphology of the Normal Cell. Biol. Bull. **169**, 449-457
6. Murer, E.H., Levin, J. and Holme, R. (1975) Isolation and Studies of the Granules of the Amebocytes in Limulus polyphemus, the Horseshoe Crab. J. Cell. Physiol. **86**, 533-542
7. Ornberg, R.L. and Reese, T.S. (1981) Beginning of Exocytosis Captured by Rapid-freezing of Limulus Amebocytes. J. Cell. Biol. **90**, 40-54
8. Young, N.S., Levin, J. and Prendergast, R.A. (1972) An Invertebrate Coagulation System Activated by Endotoxin: Evidence for Enzymatic Mediation. J. Clin. Invest. **51**, 1790-1797
9. Nakamura, S. and Levin, J. (1982) Fractionation of Limulus Amebocyte Lysate. Characterization of Activation of the Proclotting Enzyme by an Endotoxin-mediated Activator. Biochim. Biophys. Acta **707**, 217-225
10. Nakamura, S. and Levin, J. (1982) Endotoxin-mediated Limulus Proclotting Enzyme Activator and Detection of a Previously Undescribed Protease (Protease N). Biochem. Biophys. Res. Commun. **108**, 1619-1623
11. Torano, A.E., Nakamura, S. and Levin, J. (1984) Properties of the Clotting Enzyme Responsible for

Endotoxin-mediated Limulus Coagulation. Thromb. Res. **34**, 407-417

12. Nakamura, T., Morita, T. and Iwanaga, S. (1986) Lipopolysaccharide-sensitive Serine-protease Zymogen (Factor C) Found in Limulus Hemocytes. Isolation and Characterization. Eur. J. Biochem. **154**, 511-521

13. Nakamura, T., Horiuchi, T., Morita, T. and Iwanaga, S. (1986) Purification and Properties of Intracellular Clotting Factor, Factor B, from Horseshoe Crab (Tachypleus tridentatus) hemocytes. J. Biochem. **99**, 847-857

14. Nakamura, T., Morita, T. and Iwanaga, S. (1985) Intracellular Proclotting Enzyme in Limulus (Tachypleus tridentatus) Hemocytes: its Purification and Properties. J. Biochem. **97**, 1561-1574

15. Holme, R. and Solum, N.O. (1973) Electron Microscopy of the Gel Protein Formed by Clotting of Limulus polyphemus Hemocyte Extracts. J. Ultrastruct. Res. **44**, 329-338

16. Timasheff, S.N. (1981) The Self-Assembly of Long Rodlike Structures. in: Protein-Protein Interactions, (Frieden, C. and Nichol L.W., eds.) John Wiley and Sons, New York, pp. 315-336.

17. Oosawa, F. and Kasai, M. (1962) A Theory of Linear and Helical Aggregations of Macromolecules. J. Mol. Biol. **4**, 10-21

18. Timasheff, S.N. (1978) Physical Aspects of Protein Interactions, Elsevier North-Holland, Amsterdam, pp. 219-273

19. Hantgan, R.R. and Hermans, J. (1979) Assembly of Fibrin: A Light Scattering Study. J. Biol. Chem. **254**, 11272-11281

20. Castellano, G.W. (1983) Physical Chemistry, 3rd Ed., Addison-Wesley Publishing Co., Reading, MA, pp. 435-436

21. Ferry, J. (1957) Phase Changes and Dimensional Changes in Fibrinogen and Fibrin J. Cell. Comp. Physiol. **49**, 185-197

22. Hermans, J. and McDonagh, J. (1982) Fibrin: Structure and Interactions. Semin. Thromb. Hemostas. **8**, 11-24

23. Hantgan, R.R., Fowler, W., Erickson, H. and Hermans, J. (1980) Fibrin Assembly: A Comparison of Electron Microscopy and Light Scattering Results. Thromb. Haemostas. **44**, 119-124

24. Shishikura, F., Nakamura, S., Takahashi, K. and Sekiguchi, K. (1983) Coagulogens from Four Living Species of Horseshoe Crab (Limulidae): Comparison of Their Biochemical

- and Immunochemical Properties. J. Biochem. **94**, 1279-1287
25. Laemmli, U.K. (1970) Cleavage of Structural Proteins during the Assembly of the Head of Bacteriophage T4. Nature (London) **227**, 680-685
26. Solum, N.O. (1973) The Coagulogen of Limulus polyphemus Hemocytes. A Comparison fo the Clotted and Non-clotted forms of the molecule. Thromb. Res. **2**, 55-70
27. Nakamura, S., Iwanaga, S., Harada, T. and Niwa, M. (1976) A Clottable Protein (Coagulogen) from Amoebocyte Lysate of Japanese Horseshoe Crab (Tachypleus tridentatus). J. Biochem. **80**, 1011-1021
28. Williams, R.C.Jr. (1972) A Laser Light Source for the Analytical Ultracentrifuge. Anal. Biochem. **48**, 164-171
29. Yphantis, D.A. (1964) Equilibrium Ultracentrifugation of Dilute Solutions. Biochem. **3**(3), 297-317
30. Yphantis, D.A. and Waugh, D.F. (1956) Ultracentrifugal Characterization by Direct Measurement of Activity. I. Theoretical. J. Phys. Chem. **60**, 623-629
31. Johnson, M.L., Correia, J.C., Yphantis, D.A. and Halvorson, H.R. (1981) Analysis of Data from the Analytical Ultracentrifuge by Nonlinear Least-squares Techniques. Biophys. J. **36**, 575-588
32. Laue, T.M., Johnson, A.E., Esmon, C.T., and Yphantis, D.A. (1984) Structure of Bovine Blood Coagulation Factor Va. Determination of the Subunit Associations, Molecular Weights, and Asymmetries by Analytical Ultracentrifugation. Biochem. **23**, 1339-1348
33. Chervenka, C.H. (1870) A Manual of Methods for the Analytical Ultracentrifuge, Spinco Division of Beckman Instruments, Inc., Palo Alto, pp. 23-33
34. Harrington, W.F. (1975) The Effects of Pressure in Ultracentrifugation of Interacting Systems. Fractions 1, 10-18
35. Van Holde, K.E. (1985) Physical Biochemistry, 2nd Ed., Prentice-Hall, Inc., Englewood Cliffs, CA, pp. 110-121
36. Williams, J.W., Van Holde, K.E., Baldwin, R.L. and Fujita, H. (1958) The Theory of Sedimentation Analysis. Chem. Rev. **58**, 715-806
37. Weast, R.C., Astle, M.J., and Beyer, W.H. (eds.) (1986)

CRC Handbook of Chemistry and Physics, 67th Ed., CRC Press, Inc. Boca Raton, FL, pp. D219-D269

38. Teller, D.C. (1973) Characterization of Proteins by Sedimentation Equilibrium in the Analytical Ultracentrifuge. Methods Enzymol. **27**, 346-441

39. McMeekin, T.L. and Marshall, K. (1952) Specific Volumes of Proteins and the Relationship to their Amino Acid Contents. Science (Washington, D.C.) **116**, 142-143

40. Cantor, C.R. and Shimmel, P.R. (1980) Biophysical Chemistry. Part II: Techniques for the Study of Biological Structure and function, W.H. Freeman and Co., New York, pp. 550-555

41. Kumosinski, T.F. and Pessen, H. (1985) Structural Interpretation of Hydrodynamic Measurements of Proteins in Solution through Correlations with X-ray Data. Methods Enzymol. **117**, 154-182

42. Cantor, C.R. and Shimmel, P.R. (1980) Biophysical Chemistry. Part II: Techniques for the Study of Biological Structure and function, W.H. Freeman and Co., New York, Table 10-2, p. 561

43. Miyata, T., Hiranaga, M., Umezu, M. and Iwanaga, S. (1983) The Complete Amino Acid Sequence of Coagulogen Isolated from Limulus polyphemus amebocytes. in: Molecular Biology of Fibrinogen and Fibrin (Mosesson, M.W. and Doolittle, R.F., eds.) The New York Academy of Sciences, New York, pp 651-654

44. Svedberg, T. and Pedersen, K.O. (1959) The Ultracentrifuge, Johnson Reprint Corp., New York, pp 29-34

45. Nakamura, S., Shishikura, F., Iwanaga, S., and Takagi, T., Takahashi, K., Niwa, M, and Sekiguchi, K. (1980) Horseshoe Crab Coagulogens: Their Structure and Geleation Mechanism. in: Frontiers in Protein Chemistry (Liu, T.Y. et al, eds.), Elsevier North Holland, Inc, New York, pp. 495-514

46. de la Torre, J.G. and Bloomfield, V.A. (1981) Hydrodynamic Properties of Complex, Rigid, Biological Macromolecules: Theory and Applications. Quar. Rev. Biophys. **14**, 81-139

47. Tanford, C. (1961) Physical Chemistry of Macromolecules, John Wiley and Sons, Inc., New York, p. 560.

48. Edsall, J.T. and Wyman, J. (1958) Biophysical Chemistry Vol. I, Academic Press, New York, pp. 452-464

49. Craig, P.A., Olson, S.T. and Shore, J.D. (1989) Transient Kinetics of Heparin-catalyzed Protease Inactivation by Antithrombin III. J. Biol. Chem. **264**, 5452-5461
50. Armstrong, P.B., Rossner, M.T. and Quigley, J.P. (1985) An α 2-Macroglobulinlike Activity in the Blood of Chelicerate and Mandibulate Arthropods. J. Exp. Zool. **236**, 1-9
51. Koide, T. and Ikenaka, T. (1973) Studies on Soybean Trypsin Inhibitors: III. Amino-acid Sequence of the Carboxyl-terminal Region and the Complete Amino-acid Sequence of Soybean Trypsin Inhibitor (Kunitz). Eur. J. Biochem. **32**, 417-431
52. Bartelt, D.C., Shapanka, R. and Greene, L.J. (1977) The Primary Structure of the Human Pancreatic Trypsin Inhibitor: Amino Acid Sequence of the Reduced s-Aminoethylated Protein. Arch. Biochem. Biophys. **179**, 189-199
53. Ramesh, N., Sugumaran, M. and Mole, J.E. (1988) Purification and Characterization of Two Trypsin Inhibitors from the Hemolymph of Manduca sexta Larvae. J. Biol. Chem. **263**, 11523-11527
54. Armstrong, P.B. and Quigley, J.P. (1985) Proteinase Inhibitory Activity Released from the Horseshoe Crab Blood Cell During Exocytosis. Biochim. Biophys. Acta **827**, 453-459
55. Armstrong, P.B., Levin, J. and Quigley, J.P. (1984) Role of Endogenous Proteinase Inhibitors in the Regulation of the Blood Clotting System of the Horseshoe Crab, Limulus polyphemus. Thromb. Haemostas. (Stuttgart) **52(2)**, 117-120
56. Spitz, H.D. (1973) A New Approach for Sample Preparation of Protein Hydrolyzates for Amino Acid Analysis. Anal. Biochem. **56**, 66-73
57. Andrews, P.C. and Dixon, J.E. (1987) A Procedure for in situ Alkylation of Cystine Residues on Glass Fiber prior to Protein Microsequence Analysis. Anal. Biochem. **161**, 524-528
58. Laue, T.M. and Yphantis, D.A. (1979) Rapid Automatic Measurement of Rayleigh Interferograms from the Ultracentrifuge. Biophys. J. **25**, 164a
59. Laue, T.M. (1981) Rapid Precision Interferometry for the Analytical Ultracentrifuge. Ph.D. Dissertation, Univ. of Connecticut, Storrs, CT
60. Arnon, R. (1970) Papain. Methods Enzymol. **XIX**, 226-244

61. Fairbanks, G., Steck, T.L. and Wallach, D.F.H. (1971) Electrophoretic Analysis of the Major Polypeptides of the Human Erythrocyte Membrane. Biochem. **10**, 2606-2617
62. Gander, J.E. (1984) Gel Protein Stains: Glycoproteins. Methods Enzymol. **104**, 447-451
63. Protein Identification Resource, National Biomedical Research Foundation, Georgetown University Medical Center, 3900 Reservoir Rd. NW. Washington, D.C. 20007
64. Cornish-Bowden, A. (1983) Relating Proteins by Amino Acid Composition. Methods Enzymol. **91**, 60-75
65. Quigley, J.P. and Armstrong, P.B. (1985) A Homologue of α 2-Macroglobulin Purified from the Hemolymph of the Horseshoe Crab Limulus polyphemus. J. Biol. Chem. **260**, 12715-12719
66. Ritonja, A., Meloun, B. and Gubensek, F. (1983) The Primary Structure of Vipera ammodytes Venom Trypsin Inhibitor I. Biochim. Biophys. Acta **748**, 429-435
67. Bartelt, D.C. and Greene, L.J. (1971) The Primary Structure of the Porcine Pancreatic Secretory Trypsin Inhibitor I. J. Biol. Chem. **246**, 2218-2229
68. Yamamoto, M., Hara, S. and Ikenaka, T. (1983) Amino Acid Sequences of Two Trypsin Inhibitors from Winged Bean Seeds (Psophocarpus tetragonolobus (L)DC.). J. Biochem. **94**, 849-863
69. Cechova, D., Jonakova, V. and Sorm, F. (1971) Primary Structure of Trypsin Inhibitor from Cow Colostrum (Component B2). Coll. Czech. Chem. Commun. **36**, 3342-3357
70. Takahashi, H., Iwanaga, S., Kitagawa, T., Hokama, Y. and Suzuki, T. (1974) Snake Venom Proteinase Inhibitors II. Chemical Structure of Inhibitor II Isolated from the Venom of Russell's Viper (Vipera russelli). J. Biochem. **76**, 721-733
71. Winnard, P.T. (1987) Equilibrium Sedimentation of Lubrol-solubilized Rabbit Thrombomodulin. MS Thesis, Univ. of New Hampshire, Durham, NH, pp.60
72. Freifelder, D. (1976) Physical Biochemistry, W.H. Freeman and Co., San Francisco, pp. 270
73. Cantor, C.R. and Shimmel, P.R. (1980) Biophysical Chemistry. Part II: Techniques for the study of biological structure and function, W.H. Freeman and Co., New York pp. 591-601